



2-Sulfonylpyrimidines as Privileged Warheads for the Development of *S. aureus* Sortase A Inhibitors

Fabian Barthels¹, Jessica Meyr², Stefan J. Hammerschmidt¹, Tessa Marciniak³, Hans-Joachim Räder⁴, Wilma Ziebuhr³, Bernd Engels² and Tanja Schirmeister^{1*}

¹Institute for Pharmaceutical and Biomedical Sciences, Johannes Gutenberg-University, Mainz, Germany, ²Institute of Physical and Theoretical Chemistry, Julius-Maximilians-University of Würzburg, Würzburg, Germany, ³Institute for Molecular Infection Biology, Julius-Maximilians-University of Würzburg, Würzburg, Germany, ⁴Max Planck Institute for Polymer Research, Mainz, Germany

Staphylococcus aureus is one of the most frequent causes of nosocomial and community-acquired infections, with emerging multiresistant isolates causing a significant burden to public health systems. We identified 2-sulfonylpyrimidines as a new class of potent inhibitors against *S. aureus* sortase A acting by covalent modification of the active site cysteine 184. Series of derivatives were synthesized to derive structure-activity relationship (SAR) with the most potent compounds displaying low micromolar K_i values. Studies on the inhibition selectivity of homologous cysteine proteases showed that 2-sulfonylpyrimidines reacted efficiently with protonated cysteine residues as found in sortase A, though surprisingly, no reaction occurred with the more nucleophilic cysteine residue from imidazolinium-thiolate dyads of cathepsin-like proteases. By means of enzymatic and chemical kinetics as well as quantum chemical calculations, it could be rationalized that the S_NAr reaction between protonated cysteine residues and 2-sulfonylpyrimidines proceeds in a concerted fashion, and the mechanism involves a ternary transition state with a conjugated base. Molecular docking and enzyme inhibition at variable pH values allowed us to hypothesize that in sortase A this base is represented by the catalytic histidine 120, which could be substantiated by QM model calculation with 4-methylimidazole as histidine analog.

Keywords: covalent inhibition, sortase, quantum mechanics, anti-virulence, drug discovery

1 INTRODUCTION

The emergence of bacterial strains resistant to antibiotic therapy is one of the greatest medical challenges of our time. In addition to conventional antibiotics, there are efforts to develop drugs that can interfere with the virulence mechanisms of bacteria to reduce their pathogenicity (Allen et al., 2014; Dickey et al., 2017). The cysteine transpeptidase sortase A (SrtA) has been discussed as an anti-virulence drug target for nearly 20 years since SrtA mediates the attachment of virulence-associated surface proteins to the bacterial cell wall (Perry et al., 2002). It was shown that the *S. aureus* Δ SrtA knock-out mutant is attenuated in mouse infection models compared to the wild type (Mazmanian et al., 2000; Weiss et al., 2004). Neither genetic deletion (Mazmanian et al., 1999) nor selective chemical inhibition (Cascioferro et al., 2014; Zhang et al., 2014; Mu et al., 2018) of *S. aureus* SrtA was found to affect the growth properties of bacterial cells, thus deducing a lower selective pressure for resistance development compared to bactericidal antibiotics.

OPEN ACCESS

Edited by:

Jerônimo Lameira,
Federal University of Pará, Brazil

Reviewed by:

Martin D. Witte,
University of Groningen, Netherlands
Steven Verhelst,
KU Leuven, Belgium

*Correspondence:

Tanja Schirmeister
schirmei@uni-mainz.de

Specialty section:

This article was submitted to
Biological Modeling and Simulation,
a section of the journal
Frontiers in Molecular Biosciences

Received: 29 October 2021

Accepted: 03 December 2021

Published: 03 January 2022

Citation:

Barthels F, Meyr J,
Hammerschmidt SJ, Marciniak T,
Räder H-J, Ziebuhr W, Engels B and
Schirmeister T (2022) 2-
Sulfonylpyrimidines as Privileged
Warheads for the Development of *S.*
aureus Sortase A Inhibitors.
Front. Mol. Biosci. 8:804970.
doi: 10.3389/fmolb.2021.804970

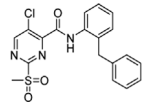
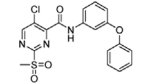
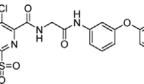
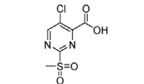
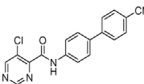
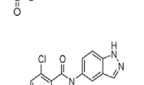
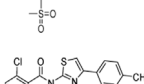
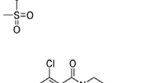
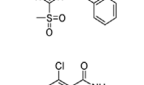
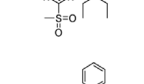
At the bacterial cell wall, virulence-associated surface proteins with C-terminal LPXTG-tagged sorting signals (e.g., protein A, fibronectin-binding proteins, clumping factors) are cleaved between threonine and glycine by the membrane-anchored SrtA and subsequently ligated to the pentaglycine tail of the peptidoglycan layer to yield covalent attachment of these surface proteins (Tsompanidou et al., 2012; Schneewind and Missiakas, 2019). The fact that SrtA plays a key role in the pathogenesis of *S. aureus* and the enzyme is drug-accessible on the outside of the bacterial cell membrane makes SrtA seemingly a well-druggable target for the development of anti-virulence agents (Cascioferro et al., 2015).

However, the privileged position of SrtA is protected from pharmacological manipulation by several structural and biochemical properties of this enzyme. *S. aureus* SrtA is an eight-stranded β -barrel protein with three conserved catalytic residues: His¹²⁰, Cys¹⁸⁴, and Arg¹⁹⁷, each of which cannot be mutated without disrupting enzymatic functionality (Ton-That et al., 2002; Bentley et al., 2008; Clancy et al., 2010). Three SrtA characteristics were identified that complicate the development of small molecule SrtA inhibitors:

- 1) The catalytic Cys¹⁸⁴ is “reversely protonated,” which means it does not form a thiolate-imidazolium pair under physiological conditions (<0.1%) and is therefore significantly less nucleophilic than structurally related cysteine proteases such as enzymes of the papain family (Ilangoan et al., 2001; Frankel et al., 2005). Hence, covalent modification of the catalytic Cys¹⁸⁴ is inefficient with cysteine protease-specific warheads such as Michael acceptors and similar electrophiles (Ton-That and Schneewind, 1999; Scott et al., 2002; Connolly et al., 2003; Kruger et al., 2004a; Liew et al., 2004).
- 2) The active site is predominantly defined by the intrinsic flexibility of the β 6/7- and β 7/8-loops (Kappel et al., 2012). Binding of the LPXTG-substrate leads to strong protein rigidization, observable from the NMR structure, and is therefore entropically penalized, which is expressed in the substrates' high K_M value of 5.5 mM (Kruger et al., 2004b; Suree et al., 2009a).
- 3) To compensate for the low activity and the high K_M value, both the LPXTG- and the pentaglycine-substrate are co-localized with the SrtA enzyme at the bacterial outer membrane (Ton-That et al., 1999). Spatial co-localization yields high local concentrations, which cannot easily be competed with reversible-competitive inhibitors *in cellulo*. Hence, most active compounds were found to be irreversible covalent inhibitors containing an electrophilic warhead that reacts with the active-site Cys¹⁸⁴ of SrtA, such as disulfides, benzisothiazolinones, thiadiazolidine-3,5-diones, and 1,3,4-thiadiazoles (Maresso et al., 2007; Suree et al., 2009b; Zhulenkova et al., 2014; Chan et al., 2017; Wehrli et al., 2019; Barthels et al., 2020; Yang et al., 2020).

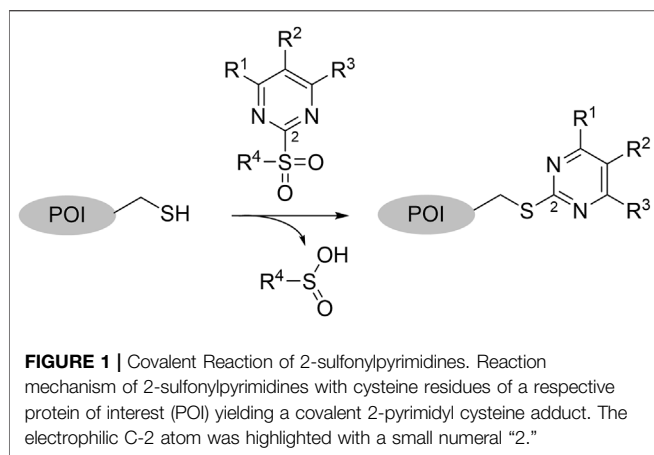
Previously, Jaudzems et al. have performed a high-throughput screening with a library of 50,000 compounds and identified 27 novel covalent modifiers of SrtA (Jaudzems et al., 2020). One of

TABLE 1 | Inhibition constants (K_i , k_{inact} , k_{2nd}) of the compounds **4** and **5a–k** for *S. aureus* SrtA; n. i. = <20% inhibition at 100 μ M.

Cpd.	Structure	K_i [μ M]	k_{inact} [s^{-1}]	k_{2nd} [$M^{-1}min^{-1}$]
4		47.1 \pm 15.7	0.00065 \pm 0.00007	870 \pm 170
5a		57.6 \pm 3.55	0.00774 \pm 0.00007	8,088 \pm 464
5b		42.37 \pm 4.62	0.00082 \pm 0.00004	1,175 \pm 67
5c			n. i.	
5d			n. i.	
5f			n. i.	
5g			n. i.	
5h			n. i.	
5i			n. i.	
5k			n. i.	

these inhibitors, parent compound sulfonylpyrimidine **4** (Table 1), showed 97% inhibition after 16 h of incubation with 100 μ M inhibitor. The irreversibility of the reaction was confirmed by 2D¹⁵N-¹H HSQC NMR, however, characterization of the inhibition kinetics and detection of the covalent adduct were still to be determined.

The use of 2-sulfonylpyrimidines as electrophilic building blocks has been documented in the synthesis of heterocyclic compounds for nearly 100 years (Sprague and Johnson, 1936). In a more biological context, heteroaromatic methyl sulfones, such as 2-methylsulfonyl benzothiazole, are well established as bioorthogonal reagents for the selective modification of non-catalytic cysteine residues (Zhang et al., 2012). Regardless of the knowledge of this potential cysteine

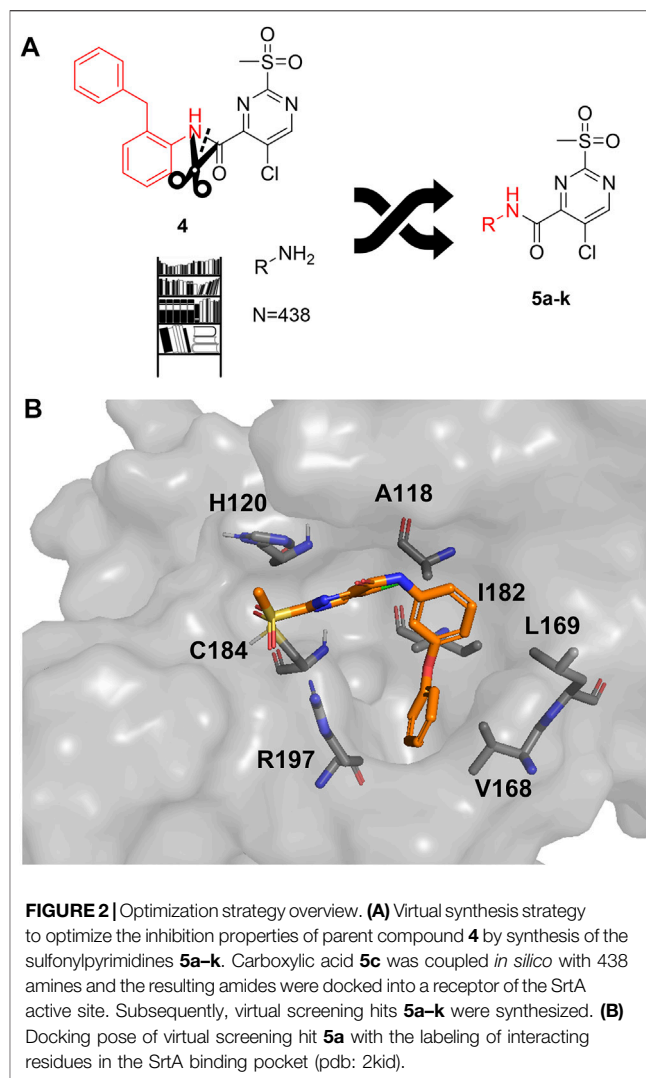


reactivity, 2-sulfonylpyrimidines have been previously considered almost exclusively as reversible modulators of pharmacological targets during drug design campaigns. Besides the studies by Jaudzems et al., 2-sulfonylpyrimidines have just recently come into the spotlight for mechanistic studies of irreversible inhibition. In the last few years, four independent studies identified 2-sulfonylpyrimidines as covalent and pharmacologically active modifiers of the following disease-associated protein targets: p53 (Bauer et al., 2016), kinesin HSET (Förster et al., 2019), succinate dehydrogenase subunit B (Li L. et al., 2017), and *S. mansoni* thioredoxin glutathione reductase (Lyu et al., 2020). All these targets share a covalently addressed cysteine residue, that is not catalytically activated and thus predominantly protonated under physiological conditions (Hallenbeck et al., 2017).

A preference for the reactivity with protonated thiols is also reflected in the ability of sulfonylpyrimidine-mediated glutathione depletion in a cellular context (Bauer et al., 2016; Wilke et al., 2018). However, compared to other electrophilic warheads, which react quantitatively with protonated cysteine residues under physiological conditions, the second-order rate constant ($60\text{--}200\text{ M}^{-1}\text{min}^{-1}$) is lower by a factor of 10–1,000 and thus 2-sulfonylpyrimidines may have the potential to be mild enough to achieve favorable target vs. off-target selectivity (Schoonen et al., 2005; Böhme et al., 2009; Chipinda et al., 2010; Wilke et al., 2018).

2-Sulfonylpyrimidines react with thiols under nucleophilic aromatic substitution (S_NAr) to form the respective pyrimidyl thioether and release the corresponding sulfinate (Bauer et al., 2016). Electron-withdrawing substituents on the aromatic ring ($R^1\text{--}R^3$) increase the polarization of the electrophilic C-2 atom and generally lead to higher reaction rates (Buděšínský and Vavřina, 1972). A schematic representation of the reaction mechanism between 2-sulfonylpyrimidines and proteinogenic cysteine residues is shown in **Figure 1**.

In this work, evidence of the covalent modification by 2-sulfonylpyrimidines, as well as the characterization of the SrtA inhibition kinetics were conducted in following up on the previously reported parent compound **4** (Jaudzems et al., 2020). Further, by using methods from molecular biology, enzyme kinetics, and quantum chemical calculations, we

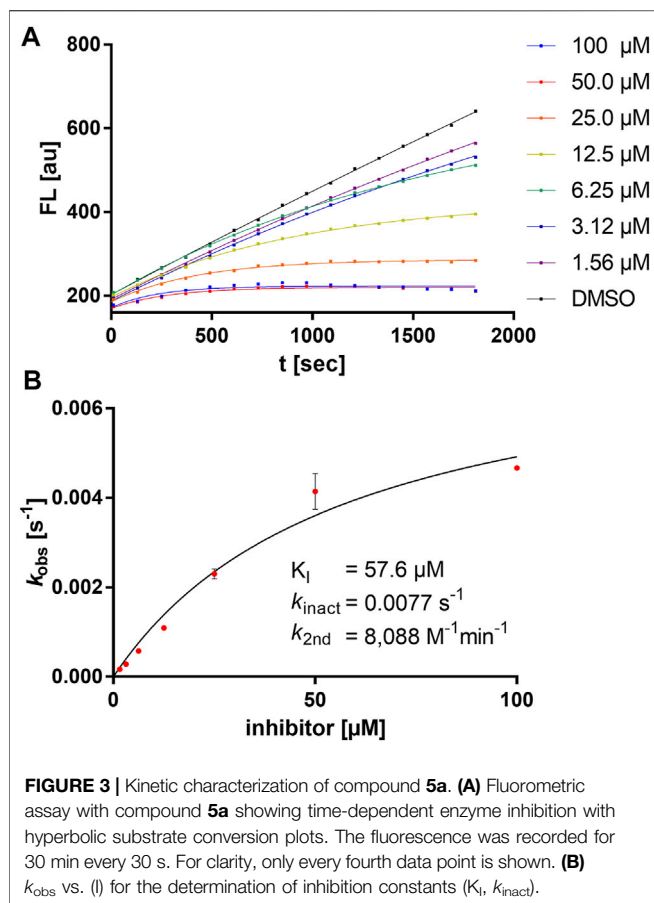


aimed to elucidate the underlying reaction mechanism of the 2-sulfonylpyrimidine warhead with cysteine residues, which might help to explain the mild yet efficient reactivity towards protonated thiols.

2 RESULTS AND DISCUSSION

2.1 Kinetic Characterization and Inhibitor Optimization Strategy

To evaluate the inhibition potency of the parent sulfonylpyrimidine **4**, this compound was tested by means of a fluorometric enzyme assay with recombinantly expressed *S. aureus* SrtA (Schmohl et al., 2017b) and Abz-LPETG-Dap (Dnp)-OH as substrate. Parent compound **4** was found to act as a time-dependent and irreversible inhibitor, which is in agreement with the literature data (Lit.: 97% inhibition after 16 h of incubation with 100 μM inhibitor; Jaudzems et al., 2020). To verify the irreversible mode of inhibition, we determined the maximum inactivation rate k_{inact} , the



dissociation constant of the reversible enzyme-inhibitor complex K_I , and the second-order rate of inhibition $k_{2\text{nd}}$. For compound **4**, a $k_{\text{inact}} = 0.00065 \text{ s}^{-1}$ was found, which is very low compared to other covalent SrtA inhibitors (Chan et al., 2017; Barthels et al., 2020; Jaudzems et al., 2020). The K_I value was as high as $47.1 \mu\text{M}$, thus, we decided to increase the potency of the sulfonylpyrimidine inhibitors by rational optimization before conducting mechanistic studies of this new inhibitor class.

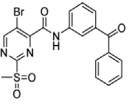
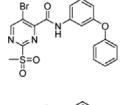
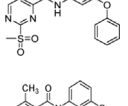
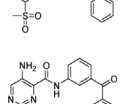
In order to increase the affinity of the sulfonylpyrimidine inhibitors, a first strategy was applied to optimize the recognition sequence while maintaining the warhead functionality. Previously, we have performed a recognition sequence optimization study on disulfanylbenzamide SrtA inhibitors (Barthels et al., 2020). Therefore, we designed and tested two chimeric inhibitors (**5b,c** **Supplementary Figure S1**). In general, sulfonylpyrimidines were synthesized based on multi-step procedures according to literature protocols. Detailed synthesis instructions can be found in the supporting information. Briefly, 2-(methanesulfonyl)pyrimidinecarboxylic acids (**2a–d**) were coupled to various commercially available or synthesized amines (**1a–o**) in the presence of 2-(1*H*-benzotriazole-1-yl)-1,1,3,3-tetramethylammonium tetrafluoroborate (TBTU) to provide the inhibitor scaffold precursors (**3a–z**). The potential sulfonylpyrimidine inhibitors (**4**, **5a–k**, **6a–n**, **7a–e**) were subsequently synthesized by oxidation with potassium peroxymonosulfate (Webb, 1994).

TABLE 2 | Inhibition constants (K_I , k_{inact} , $k_{2\text{nd}}$) of the compounds **6a–n** for *S. aureus* SrtA; n. i. = <20% inhibition at $100 \mu\text{M}$.

Cpd.	Structure	K_I [μM]	k_{inact} [s^{-1}]	$k_{2\text{nd}}$ [$\text{M}^{-1}\text{min}^{-1}$]
6a		29.6 ± 9.39	0.00986 ± 0.00128	$20,785 \pm 4,074$
6b		47.5 ± 4.62	0.00578 ± 0.00033	$7,305 \pm 294$
6c		78.8 ± 9.92	0.00864 ± 0.00092	$6,593 \pm 243$
6d		60.3 ± 6.40	0.00618 ± 0.00025	$6,181 \pm 489$
6e		—	—	882 ± 43
6f		—	—	588 ± 48
6g		—	—	n. i.
6h		—	—	n. i.
6i		—	—	n. i.
6k		—	—	n. i.
6l		—	—	n. i.
6m		—	—	n. i.
6n		—	—	n. i.

The chimeric 3-phenoxyphenyl glycine derivative (**5b**) showed slightly higher overall inhibition potency ($k_{2\text{nd}} = 1,175 \text{ M}^{-1}\text{min}^{-1}$) than parent compound **4** (**Table 1**). In contrast, the adapted fragment inhibitor (**5c**) showed no SrtA inhibition even at a final inhibitor concentration of $300 \mu\text{M}$. From the inhibition results, we concluded that the binding geometry of the previously optimized disulfanylbenzamide recognition sequence (**5b**, **Supplementary Figure S1**) is probably not optimally transferable to the novel sulfonylpyrimidine derivatives because of the different aromatic substitution pattern of the warheads' electrophilic center (ortho vs. meta).

TABLE 3 | Inhibition constants (K_i , k_{inact} , k_{2nd}) of the compounds **7a–e** for *S. aureus* SrtA; n. i. = <20% inhibition at 100 μ M.

Cpd.	Structure	K_i (μ M)	k_{inact} (s^{-1})	k_{2nd} ($M^{-1}min^{-1}$)
7a		32.0 ± 5.07	0.01493 ± 0.00132	$28,185 \pm 2,117$
7b		55.9 ± 11.6	0.01285 ± 0.00147	$13,998 \pm 1,462$
7c		33.8 ± 11.2	0.00239 ± 0.00047	$4,364 \pm 596$
7d		—	—	$1,204 \pm 139$
7e			n. i.	

As a second attempt, we tried an *in silico* supported optimization approach (**Figure 2A**): Using virtual synthesis, we combined the warhead function of parent compound **4** with our in-house inventory of aliphatic and aromatic amines ($N = 438$). Subsequently, molecular docking to the binding pocket of SrtA was carried out using the Glide docking algorithm (Friesner et al., 2004). Potential binders were discriminated in this virtual screening approach by a distance scan of the electrophilic C-2 atom in the pyrimidine ring from the catalytic Cys¹⁸⁴ in the binding pocket. Structures that showed a distance of less than 5 Å were sorted according to their docking score and manual inspection of the binding pose. The seven best sulfonylpyrimidines were synthesized for *in vitro* evaluation (**5a,d–k**).

The exchange of the 2-benzylaniline fragment (**4**) for the 3-phenoxyaniline fragment (**5a**) led to a significant improvement of the overall inhibition potency by a factor of 10 (**Table 1**, $k_{2nd} = 8,088 M^{-1}min^{-1}$). The docking pose of **5a** with putative interactions in the SrtA binding pocket can be seen in **Figure 2B**. Here, the sulfonylpyrimidine warhead is positioned orthogonally to the axis of the three catalytic residues (His¹²⁰, Cys¹⁸⁴, Arg¹⁹⁷) and is thus reasonably positioned for a nucleophilic attack of the Cys¹⁸⁴ thiol to the pyrimidine ring. The 3-phenoxyaniline moiety fits well to the L-shaped binding pocket of SrtA and shows interactions with the hydrophobic residues (Ala¹¹⁸, Val¹⁶⁸, Leu¹⁶⁹, Ile¹⁸²) in the S3/S4 substrate binding pockets.

Exemplarily, the substrate conversion plot with time-dependent inhibition is shown in **Figure 3**. The apparent first-order rate constant (k_{obs}) in the presence of inhibitor **5a** varied hyperbolically with the concentration of the inhibitor. A limiting value was approached asymptotically at higher inhibitor

concentrations indicating two-step mechanism inactivation kinetics.

The other virtual screening hits (**5d–k**) were also assayed using the fluorometric enzyme assay at an inhibitor concentration of 100 μ M but showed no measurable inhibition of SrtA (**Table 1**). For achieving warhead selectivity towards off-targets, such a strong dependence on a recognition sequence for a covalent inhibitor might be desirable (Copeland, 2005; Awoonor-Williams and Rowley, 2018). The inhibition data and structures of the sulfonylpyrimidines **4** and **5a–k** are summarized in **Table 1**.

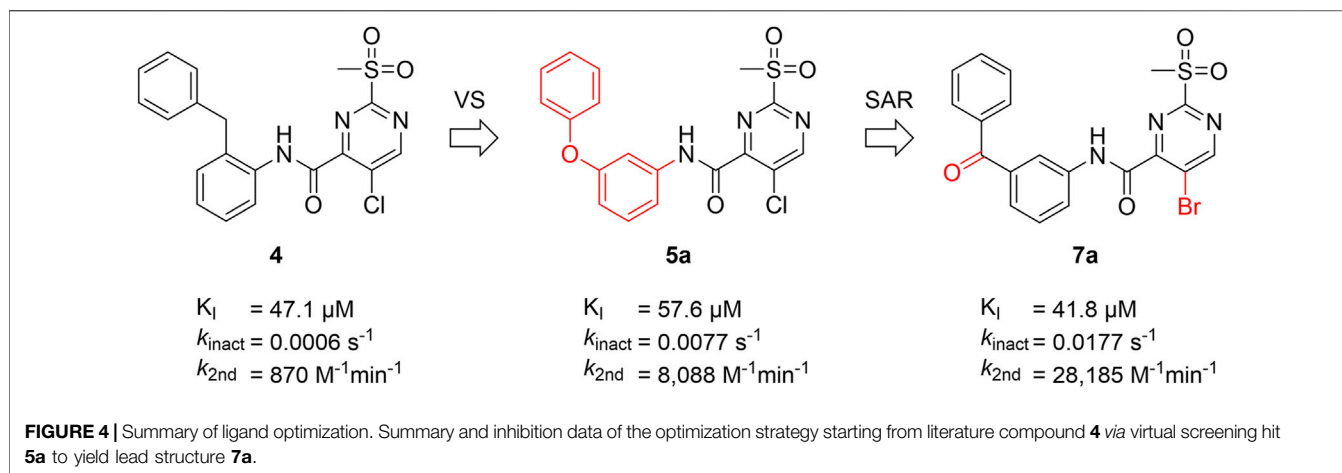
2.2 SAR Study Around Hit Compound 5a

The subtle structural transformation from 2-benzylaniline derivate (**4**) to 3-phenoxyaniline derivate (**5a**) resulted in a tenfold increase of the inhibitory potency ($k_{2nd} = 870$ vs. $8,088 M^{-1}min^{-1}$), hence, we hypothesized that the inhibitor's recognition sequence can be further systematically optimized. Therefore, we conducted a SAR study around virtual screening hit **5a**. The inhibition results of the synthesized compounds **6a–n** are shown in **Table 2**.

Six out of 13 sulfonylpyrimidines (**6a–f**) did inhibit SrtA in the fluorometric enzyme assay, but with varying potency. Strikingly, we observed a drop in SrtA inhibition for most modifications on the 3-phenoxyaniline motif. These structural “activity cliffs” highlight the importance of the accurate positioning of the warhead towards the catalytic Cys¹⁸⁴ for a successful covalent reaction (Bajorath, 2019).

Only small changes in inhibition potency were observed upon changes of the aryl ether connecting group of compound **5a** to the analogous aryl thioether (**6b**) or the methylene derivate (**6d**). However, the exchange to a ketone connecting unit (**6a**) resulted in a significant increase of inhibition potency which might be due to beneficial interactions with Arg¹⁹⁷. Based on the k_{2nd} value, compound **6a** ($k_{2nd} = 20,785 M^{-1}min^{-1}$) appeared to be 2.5-fold more potent than virtual screening hit **5a**. Alteration of the *meta*-substitution pattern resulted in the complete abolition of inhibition for the *ortho* (**6g**) and *para* (**6h**) derivatives. After truncation of the connecting group to the biphenyl derivative (**6f**), only minor inhibition potency remained ($k_{2nd} = 588 M^{-1}min^{-1}$). On the other hand, with connector elongation to the benzyl ether (**6k**) or an amide derivate (**6m**), the inhibition was completely abolished.

Modifications of the terminal phenyl ring were well tolerated in the case of an exchange to an aliphatic cyclohexyl ring (**6c**, $k_{2nd} = 6,593 M^{-1}min^{-1}$) but resulted in a severe loss of inhibition when downsized to a methoxy group (**6e**, $k_{2nd} = 882 M^{-1}min^{-1}$). Other transformations such as amide inversion at the sulfonylpyrimidine ring (**6i**), rigidization to a benzofuran derivative (**6l**), or decyclization of the central phenyl ring (**6n**) resulted in complete loss of inhibition. For derivatives **6e,f**, two-step kinetics could not be confirmed because of a lacking k_{obs} saturation at higher inhibitor concentrations. The K_i values of these compounds were estimated to be significantly higher than 100 μ M. In these cases, the inhibition potency (k_{2nd} value) was determined by Lineweaver-Burk linearization.



In addition to the modification of the recognition sequence, the chlorine substituent on the sulfonylpyrimidine ring was also varied and derivatives **7a–e** were synthesized (Table 3).

A positive correlation was found between the intensity of the electron-withdrawing properties of the substituents and the inhibition potency: Br (**7b**) > Cl (**5a**) > H (**7c**) > CH₃ (**7d**) >> NH₂ (**7e**). The increase in inhibition was mainly caused by an increase in the k_{inact} value and was not due to affinity changes for the target (K_I value). The electronic effects of the substituents on the pyrimidine ring predominantly influenced the warhead reactivity, which can be quantified and is discussed by the analysis of the Hammett constants (Section 2.7). In summary, starting from virtual screening hit **5a**, two SAR transformations proved to be beneficial: Conversion of the aryl ether connecting group to the ketone derivative **6a** and the halogen exchange at the pyrimidine ring from chlorine to bromine derivative **7b**. Subsequently, the two modifications were combined and inhibitor **7a** was synthesized. Considering the $k_{2\text{nd}}$ value, **7a** was the most potent irreversible inhibitor of this study ($k_{2\text{nd}} = 28,185 \text{ M}^{-1}\text{min}^{-1}$). The optimization strategy is summarized in Figure 4.

2.3 Identification of Covalent Adducts by Mass Spectrometry

For electron-deficient heteroaromatic compounds, S_NAr reactions often occur at the aromatic carbon atom with the substituent representing the best leaving group (Rohrbach et al., 2019). For 2-sulfonylpyrimidines, this is generally the sulfonyl group (Buděšínský and Vavřina, 1972; Bauer et al., 2016; Förster et al., 2019). However, the scaffold used here also carried a halogen substituent which, depending on the reaction conditions, might represent the actual leaving group during organic synthesis (Buděšínský and Vavřina, 1972). Thus, we determined the point of nucleophilic thiol attack by means of ESI mass spectrometry between the reaction of compound **7a** and cysteine in phosphate buffered solution at pH 7.5. The reaction between compound **7a** (100 μM) and cysteine (100 μM) occurred quantitatively in less than 10 min to form the 2-pyrimidyl cysteine adduct ($m/z = 501.03$) as described by the mechanism

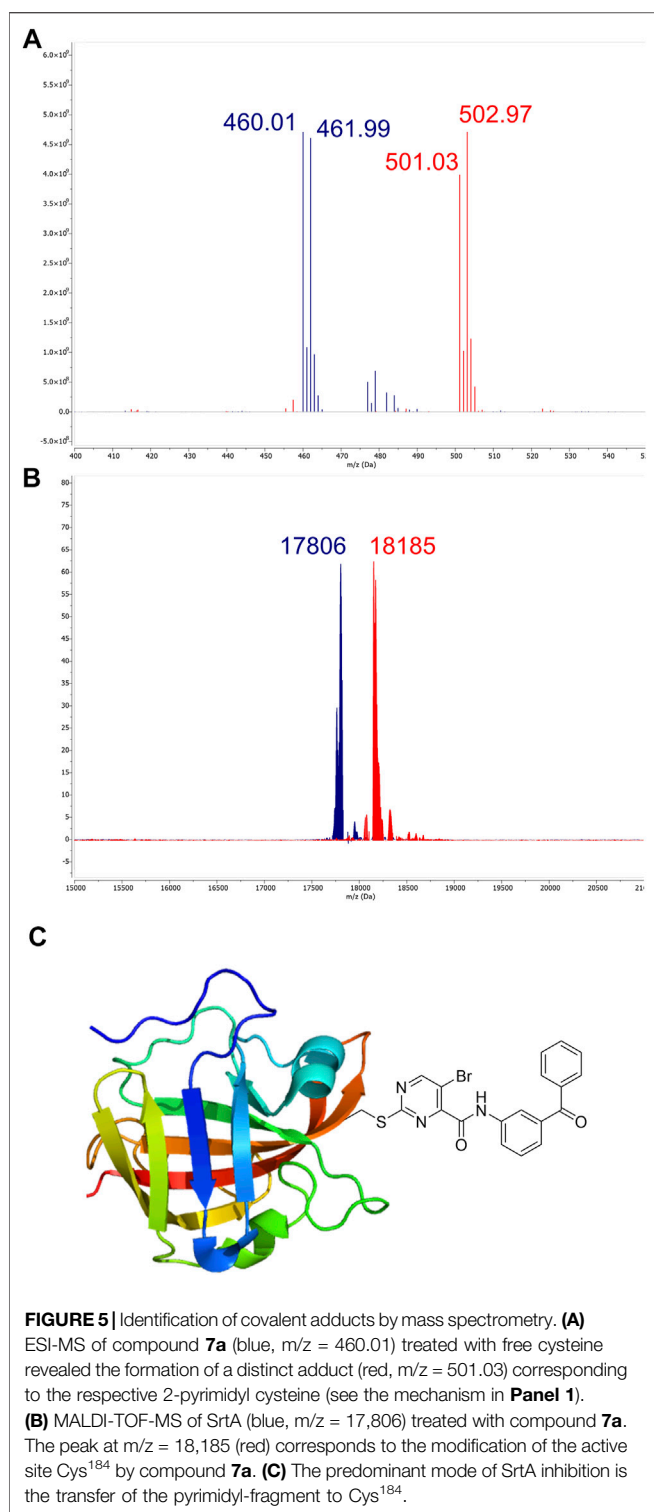
in Figure 1. As expected, the isotope pattern specific for bromine ($m/z = 502.97$) was preserved for the adduct mass (Figure 5A). Similarly, for the chlorine-substituted compound **5c**, the analogous reaction adduct could be detected by LC/MS (Supplementary Figure S2). Accordingly, it was confirmed that under physiological conditions, the sulfonyl group was the leaving group and stable 2-pyrimidyl adducts were formed.

By using MALDI-TOF mass spectrometry, we aimed to determine the mode of inhibitory action in an enzymatic context. For the native SrtA, we found a protein mass at $m/z = 17,806$. Treatment with inhibitor **7a** resulted in quantitative conversion and showed a single mass peak at $m/z = 18,185$ (Figure 5B), which matches the corresponding 2-pyrimidyl adduct and proves the covalent inhibition mechanism (Figure 5C).

2.4 Protease Inhibition Selectivity

The sulfonylpyrimidines studied in this work were characterized as mild covalent inactivators of the SrtA enzyme (Table 3 and Figure 5) and exhibited a strong scaffold dependence for their inhibitory potency (Table 2). To investigate how these sulfonylpyrimidines affect the activity of other cysteine and serine proteases, a selectivity panel was constructed from a matrix of 6 diverse sulfonylpyrimidines and 6 different proteases. The compounds were assayed at a final compound concentration of 100 μM for the cysteine proteases human cathepsin B (hCatB), cathepsin L (hCatL), and *T. brucei* rhodesain (Rd). Furthermore, the serine proteases NS2B-NS3 from Zika virus (ZIKV), the homologous protease from Dengue virus (DENV), and the human protease urokinase plasminogen activator (uPA) were tested for their susceptibility. The results of the inhibition data are summarized in Table 4.

Cathepsin B/L, rhodesain, and SrtA are all structurally related to papain-like proteases, thus, we used their relatedness to study the selectivity of our inhibitors (Bradshaw et al., 2015). The selected sulfonylpyrimidines appear to have good selectivity for SrtA, as the other three proteases were inhibited at most 29.4% by compound **6g**. A time-dependent inhibition, as with SrtA, could not be observed over the measurement duration of 30 min, which leads to the



conclusion that sulfonylpyrimidines probably do not react covalently with cathepsin-related proteases.

A significant difference between cathepsin B/L, rhodesain, and SrtA is that in contrast to SrtA, the catalytically active cysteine is present in thiolate form in the first three proteases (Otto and Schirmeister, 1997; Ehmke et al., 2013; Klein et al., 2020b). This

observation seems counterintuitive at first since the reversely protonated thiol of SrtA has a lower nucleophilicity than the thiolate in cathepsin-related proteases. The reaction of electrophiles such as sulfonylpyrimidines should react favorably with the thiolate as a stronger nucleophile (Zhang et al., 2012). A theoretical examination of these observations is provided later in this study through docking and quantum chemical calculations (**Section 2.8**).

The ZIKV NS2B/NS3 protease is a serine protease and contains two non-catalytic cysteine residues, thus as expected, only <30% inhibition at 100 μM inhibitor concentration was found. The related DENV NS2B/NS3 protease has no cysteine residues in its protein sequence and was inhibited by a maximum of only 15% (Li Y. et al., 2017). The urokinase plasminogen activator, which is also a serine protease, was inhibited by less than 25% by most compounds. Compound **6g**, however, showed 67% inhibition, but this inhibition was observed to be not time-dependent and thus presumably due to reversible binding.

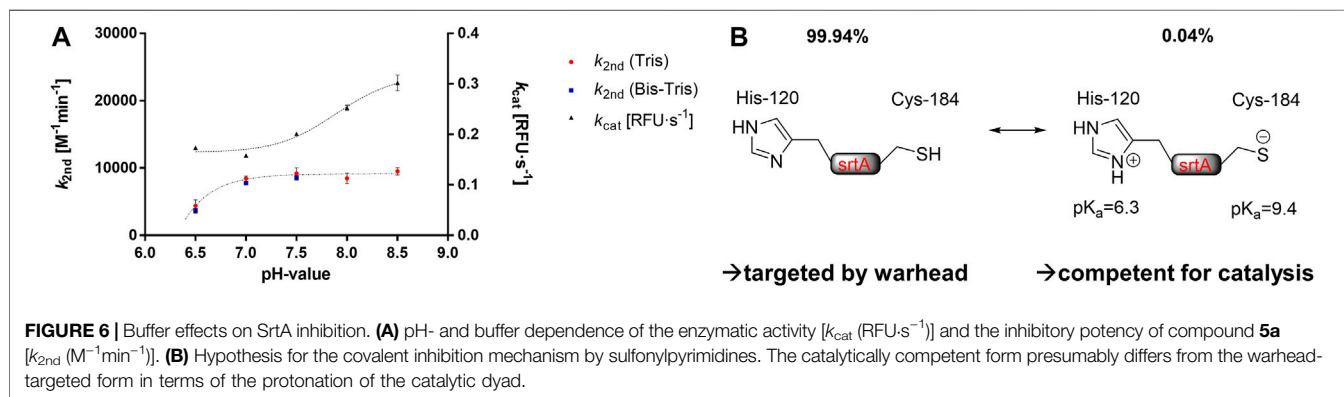
2.5 Solvent Effects on SrtA Inhibition

To investigate which thiol protomer (Cys-SH or Cys-S) of SrtA Cys¹⁸⁴ is responsible for the reaction with sulfonylpyrimidines, enzyme assays were performed at different pH values and in different enzyme buffers. It is known that the catalytic Cys¹⁸⁴ of SrtA is predominantly (99.94%) in the protonated thiol form under physiological conditions at pH 7.5 (van't Hof et al., 2015). The pK_a value was previously determined to be 9.4 by NMR titration (Connolly et al., 2003). Thus, increasing the pH value of the enzyme solution above pH 7.5 resulted in a significant increase in the thiolate species content. This on one hand led to increased enzyme activity, on the other hand, made SrtA also more vulnerable for covalent modification by electrophiles such as Michael acceptors leading to an increase in the observed rate of irreversible enzyme inactivation (Connolly et al., 2003; Frankel et al., 2005; Schmohl et al., 2015; Barthels et al., 2020). Enzyme assays were performed at five pH values between 6.5 and 8.5 in Tris or Bis-Tris buffers within the possible buffer capacities. Both the relative enzyme activity k_{cat} ($\text{RFU}\cdot\text{s}^{-1}$) of the DMSO control and the inhibition potency $k_{2\text{nd}}$ ($\text{M}^{-1}\cdot\text{min}^{-1}$) of compound **5a** were determined at each pH value (**Figure 6A**).

The observed activity increase of SrtA (k_{cat}) at pH values above pH 7.5 is in agreement with the literature (Frankel et al., 2005; Barthels et al., 2020). However, the inhibitory potency of compound **5a** showed no significant differences at varying pH values between 7.0 and 8.5. This is contrary to the inactivation kinetics of known SrtA targeting warheads, which have been shown to react preferentially with the thiolate species (Connolly et al., 2003; Frankel et al., 2005; Schmohl et al., 2015; Barthels et al., 2020). We take this, in addition to the protease selectivity results (**Table 4**), as further evidence that sulfonylpyrimidines might react preferentially with protonated thiols in this proteinogenic context (**Figure 6B**). Albeit yet unclear, we aimed to elucidate the molecular background by *in vitro* and *in silico* methods. In addition to the cationic Tris and Bis-Tris buffers, inhibition experiments of SrtA by compound **5a** were also performed in the zwitterionic HEPES buffer at pH 7.5 ($k_{2\text{nd}} = 7,956 \text{ M}^{-1}\cdot\text{min}^{-1}$). Hence, the inhibitory potency at pH 7.5 did not

TABLE 4 | Protease inhibition selectivity of a representative compound set. Compounds were tested at a final concentration of 100 μM inhibitor. The inhibition is expressed relative to the DMSO control in (%); n. i. = no inhibition at 100 μM .

Cpd	Structure	SrtA (%)	CatB (%)	CatL (%)	Rd	ZIKV (%)	DENV	uPA
5a		99.0	6.6	8.8	24.6%	6.4	n. i.	23.0%
5c		19.6	5.8	6.6	20.0%	7.7	n. i.	n. i.
6a		98.4	5.6	18.0	n. i.	18.6	5.1%	2.2%
6g		21.8	11.8	29.4	15.0%	18.3	2.6%	67.0%
6i		36.0	9.5	21.3	9.2%	29.3	15.0%	59.4%
7b		99.2	12.5	28.5	4.7%	18.3	5.2%	11.2%



differ significantly between all three investigated buffers indicating no involvement of a buffer molecule for the reaction in an enzymatic context.

In contrast, when the pH value was lowered to 6.5, a substantial decrease in SrtA inhibitory potency was observed (pH 7.0: $k_{2nd} = 8,436 \text{ M}^{-1}\text{min}^{-1}$; pH 6.5: $k_{2nd} = 4,384 \text{ M}^{-1}\text{min}^{-1}$). However, the enzymatic activity (k_{cat}) did not decrease as much with this pH change, which is in agreement with the literature reports (Zong et al., 2004). The reduction in inhibitory potency at pH < 7.0 must be due to other SrtA residues than Cys¹⁸⁴ since the proportions of the thiol/thiolate ratio do not change significantly at pH 6.5–7.0. However, the pK_a value of the neighboring His¹²⁰ is 6.3 leading to a significant protonation change when the pH is lowered from pH 7.0 to pH 6.5 (Connolly et al., 2003).

It is conceivable that the protonated imidazolium form prevents the reaction of Cys¹⁸⁴ with the sulfonylpyrimidine warhead. This would also hint at an explanation for the selectivity over the cysteine proteases with zwitterionic dyad (**Table 4**) since these have such an imidazolium ion adjacent to their catalytic cysteine residue which might prevent reversible binding to the cathepsin B/L or rhodesain binding pockets (Mladenovic et al., 2007; Ehmke et al., 2013; Paasche et al., 2014).

2.6 In-Solution Cysteine Reactivity

Next, the reaction of sulfonylpyrimidines was studied kinetically in a non-proteinogenic context with the free amino acid cysteine as a nucleophile to gather additional evidence for the reaction mechanism of sulfonylpyrimidines with thiols.

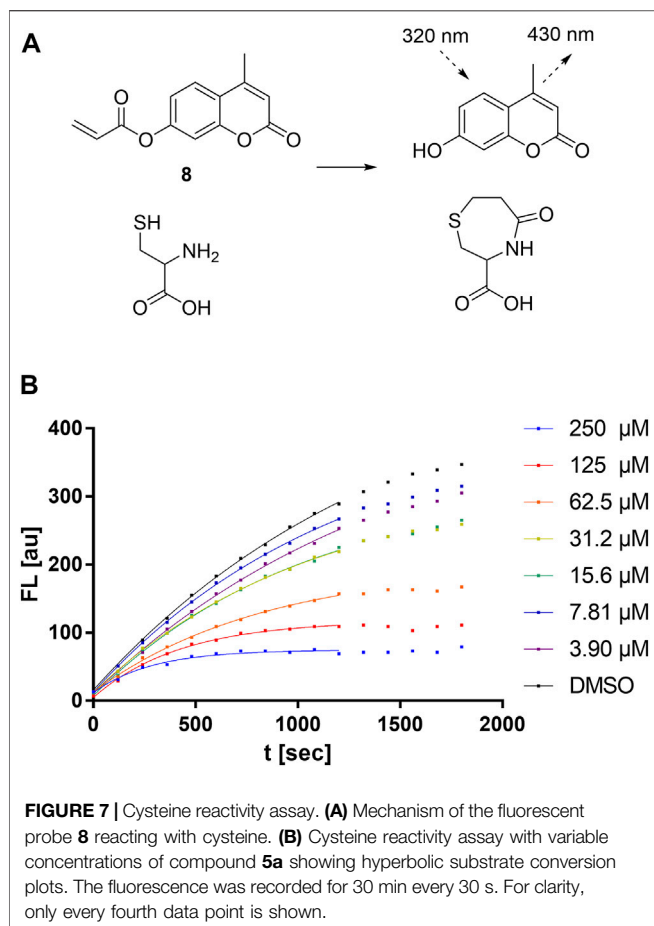


FIGURE 7 | Cysteine reactivity assay. **(A)** Mechanism of the fluorescent probe **8** reacting with cysteine. **(B)** Cysteine reactivity assay with variable concentrations of compound **5a** showing hyperbolic substrate conversion plots. The fluorescence was recorded for 30 min every 30 s. For clarity, only every fourth data point is shown.

In order to study the kinetics of sulfonylpyrimidines reacting with free cysteine in solution, a strategy for a competitive fluorescence-based assay was adapted from previous works (Epps and Taylor, 2001; Sameshima et al., 2017). For this purpose, a novel cysteine-reactive probe **8** was synthesized, which, in terms of signal-to-noise ratio, was superior to the probes used in the previous cysteine assays (Zeng et al., 2017). The reaction of probe **8** with cysteine liberates 4-methylumbelliferone as a fluorometrically detectable product (Figure 7A), and thus, the fluorescence increase can be described by the second-order rate constant k_{probe} (Equation 1).

Upon the addition of competitive and irreversible cysteine modifiers such as sulfonylpyrimidines, the fluorescence increase of the probe reaction was hyperbolically attenuated (Figure 7B). According to the conceptual deduction described previously (Epps and Taylor, 2001; Sameshima et al., 2017), the experimental fluorescence curves can be analyzed by nonlinear regression as first-order reaction progress curves (Equation 2). The parameter k_{obs} describes the curvature corresponding to the sum of the competing kinetics (Equation 3). Under the assumptions that 1) the competitive reaction between sulfonylpyrimidines vs. probe with cysteine is started by simultaneous addition, and 2) sulfonylpyrimidines are added at a much higher concentration than cysteine ($5 \mu\text{M}$) and the probe ($5 \mu\text{M}$), the k_{obs} values depend substantially on the k_{chem}

value. The compound-specific second-order inactivation parameter k_{chem} can be determined by linear regression from the k_{obs} values of the dilution series (Equation 4).

$$\frac{d[\text{FL}]}{dt} = k_{\text{probe}} [\text{Cys}] [\text{probe}] \quad (1)$$

$$\text{FL} = \frac{[\text{Cys}]_{\text{total}} \cdot k_{\text{probe}} [\text{probe}]}{k_{\text{probe}} [\text{probe}] + k_{\text{chem}} [\text{sulfonylpyrimidine}]} (1 - e^{-k_{\text{obs}} \cdot t}) \quad (2)$$

$$k_{\text{obs}} = k_{\text{chem}} [\text{sulfonylpyrimidine}] + k_{\text{probe}} [\text{probe}] \quad (3)$$

$$k_{\text{chem}} = \frac{k_{\text{obs}}}{[\text{sulfonylpyrimidine}]} \quad (4)$$

The observed k_{chem} values of a comprehensive set of sulfonylpyrimidines are shown in Table 5. Bauer et al. have already determined a k_{chem} value of compound **5c** vs. glutathione ($k_{\text{chem}} = 82 \text{ M}^{-1} \text{ min}^{-1}$). Our determined k_{chem} for the reaction of the identical compound with cysteine is $63 \text{ M}^{-1} \text{ min}^{-1}$ and thus, as expected, in the same order of magnitude. The determined k_{chem} values ranged from 6 to $104 \text{ M}^{-1} \text{ min}^{-1}$, i.e., they are 10–10,000 times lower than for the reactions of the reported Michael acceptors 1-penten-3-one, methyl propiolate, and methyl acrylate with GSH (Böhme et al., 2009). This confirms the previous reports that sulfonylpyrimidines are mild cysteine modifiers with potential application in a cellular context (Bauer et al., 2016; Li L. et al., 2017; Förster et al., 2019; Jaudzems et al., 2020).

From the kinetic constants k_{chem} (cysteine assay) and $k_{2\text{nd}}$ (SrtA inhibition), selectivity indices (S.I.) were calculated that compare how efficient the inactivation of SrtA was in comparison with the in-solution reactivity towards free cysteine (Table 5). It was found that the S.I. values do not depend on the halogen substituent, but rather on the recognition sequence: 3-benzoylaniline derivatives **6a** and **7a** were superior to 3-phenoxyaniline derivatives **5a** and **7b** in terms of the S.I. by about a factor of two. This is in agreement with findings from the enzymatic context that the recognition sequence mainly influences the affinity of binding (K_i), with the halogen substituent influencing the reaction rate (k_{inact} , k_{chem}).

Furthermore, the influence of different solvents on the reaction of sulfonylpyrimidines with thiols in solution was investigated. No reactivity was observed between cysteine and **5a** or **5c** in water/DMSO mixtures. Likewise, no reactivity was detected between **5c** and 2-phenylethanethiol in chloroform. These observations are in agreement with the literature. In organic synthesis, such reactions required a base and elevated temperature (Sprague and Johnson, 1936; Buděšinský and Vavřina, 1972). However, between **5a** and cysteine, quantitative turnover (<10 min) was observed in phosphate-buffered solution during the preparation of ESI-MS experiments (Figure 5A) and cysteine reactivity assays (Figure 7). The buffer component appeared to be essential for the reaction in an aqueous solution.

In support of this qualitative statement, a quantitative estimation of the buffer-dependent reaction between sulfonylpyrimidines and cysteine was also performed: The

TABLE 5 | Kinetic constants (k_{chem} and $k_{2\text{nd}}$) of the selected compound set investigated by the cysteine reactivity assay. Selectivity indices were calculated from $k_{2\text{nd}}/k_{\text{chem}}$.

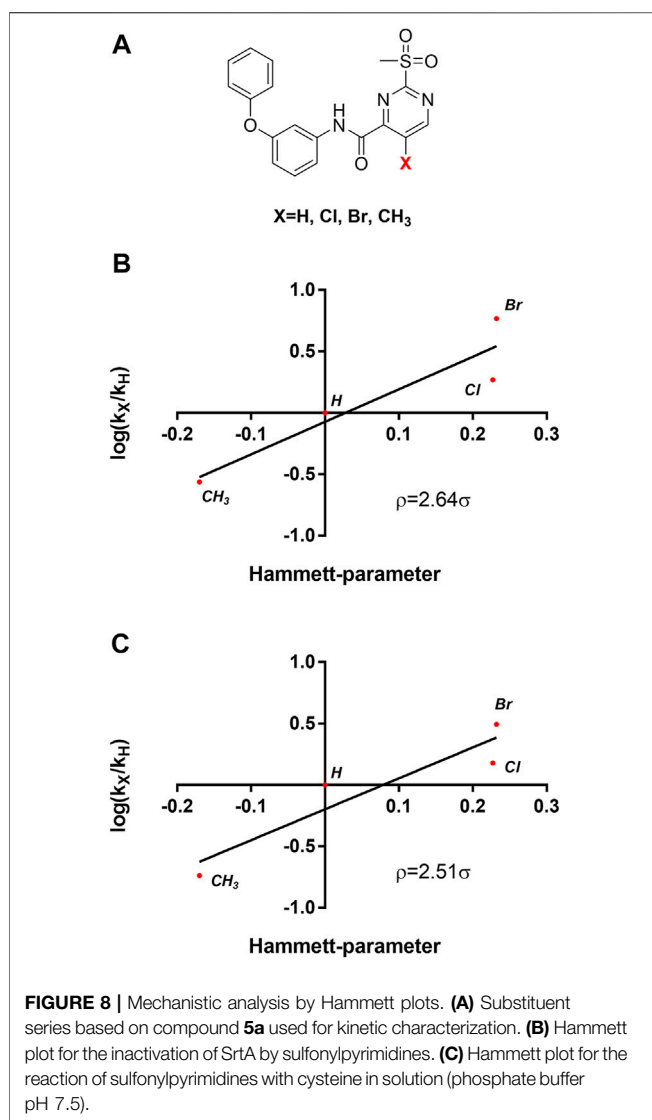
Cpd.	Structure	Cysteine k_{chem} ($\text{M}^{-1}\text{min}^{-1}$)	SrtA $k_{2\text{nd}}$ ($\text{M}^{-1}\text{min}^{-1}$)	S. I.
5a		50.8 ± 16.6	$8,088 \pm 464$	159
5c		63.0 ± 2.01	0	—
6a		63.3 ± 8.37	$20,785 \pm 4,074$	327
6i		0	0	—
7a		104.9 ± 22.5	$28,185 \pm 2,117$	268
7b		104.1 ± 19.4	$13,998 \pm 1,462$	134
7c		33.58 ± 2.93	$4,364 \pm 596$	129
7d		6.14 ± 1.71	$1,204 \pm 139$	196
7e		0	0	—

cysteine reactivity assay of compound **5c** was performed in addition to the usage of phosphate buffer ($k_{\text{chem}} = 63.0 \pm 2.01 \text{ M}^{-1}\text{min}^{-1}$) also in bicarbonate buffered solution at an identical pH 7.5. The reaction rate in bicarbonate buffer appeared to be significantly reduced ($k_{\text{chem}} = 21.9 \pm 1.27 \text{ M}^{-1}\text{min}^{-1}$). Mechanistic participation of the buffer molecule is discussed during the quantum chemical investigations (Section 2.8).

2.7 Mechanistic Evaluation by Hammett Plot Analysis

Table 3 shows that sulfonylpyrimidine derivatives, whose halogen substituent was varied, exhibited significantly different reaction rates in the inactivation of SrtA. The same was found for the cysteine reactivity assays (Table 5). If the pyrimidine ring is regarded as a pseudo-atom, according to Hammett's theory, linear logarithmic relationships can be

established between rate constants ($\text{M}^{-1}\text{min}^{-1}$) and Hammett's substituent constants (σ), which allow qualitative mechanistic conclusions to be drawn (Hammett, 1937; Flynn, 1980). For this purpose, a substituent series based on compound **5a** ($R = \text{Cl}, \text{Br}, \text{H}, \text{CH}_3$) was investigated (Figure 8A). Plotting the logarithmic-normalized second-order rate constants ($k_{2\text{nd}}, k_{\text{chem}}$) allowed us to generate Hammett plots for the reaction of sulfonylpyrimidines with SrtA (Figure 8B) and for the in-solution reaction with free cysteine (phosphate buffer pH 7.5, Figure 8C). From these, we found positive ρ values (slope) of 2.64 resp. 2.51σ , which are consistent with the rate-limiting nucleophilic attack (Kiemele et al., 2016), and strongly suggest a concerted $\text{S}_{\text{N}}\text{Ar}$ mechanism without stabilization of a Meisenheimer intermediate (Choi et al., 2009). The ρ -values obtained from enzymatic reactions and reactions with free cysteine are almost identical suggesting an analogous reaction mechanism for covalent modification of SrtA and free cysteine.



2.8 Theoretical Investigations

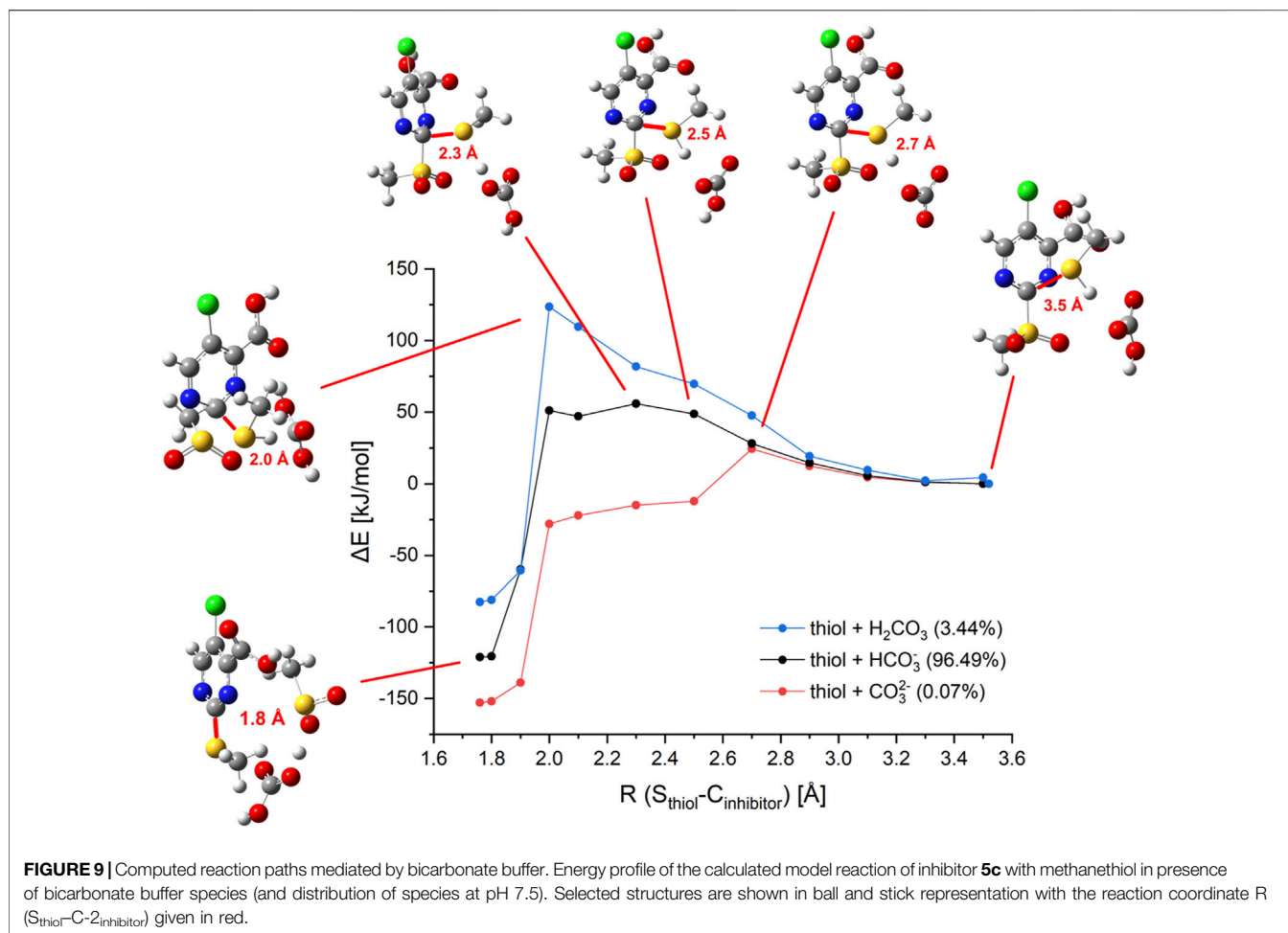
To gain insights into the mechanism of 2-sulfonylpyrimidine inhibitors in an enzymatic environment, QM/MM calculations would be desirable. However, the available X-ray structures of *S. aureus* SrtA differ strongly in the geometrical structure of their active site, and it is yet unclear which one represents the reactive conformation. Additionally, the enzyme is very flexible which makes it difficult to select appropriate conformations for the computation. Thus, unambiguous QM/MM computations were thought to be not available. Hence, we focused on the comparison of the warhead reaction in solution with the available experimental data. These findings were then applied to shed some light on the reaction of 2-sulfonylpyrimidines with SrtA. The reaction of inhibitor **5c** with methanethiol in (implicit) aqueous solution was selected as a model system. The relative orientation of the reactants together with the main reaction coordinate is depicted in **Supplementary Figure S3**. As the main reaction coordinate of the nucleophilic substitution of the sulfonyl group by the thiol (ate) we selected the distance

between the sulfur center of thiol and the C-2 atom of the inhibitor ($R_{\text{thiol-C-2}_{\text{inhibitor}}}$). To obtain single points of the corresponding reaction paths this distance was frozen while all other degrees of freedom were optimized. In the course of the calculations, only the $R_{\text{thiol-C-2}_{\text{inhibitor}}}$ distance was frozen but not the relative orientation of the two fragments to each other. Hence, the corresponding reaction path represents the minimum energy path (MEP) of the reaction. More details about the calculations are described in the experimental section.

First, the reactions of **5c** with methanethiol as well as methanethiolate were investigated. As shown in **Supplementary Figure S4**, the reaction with negatively charged methanethiolate occurs without any barrier, while the reaction with neutral methanethiol shows a barrier of 142 kJ/mol. Due to the high reaction barrier, a reaction of **5c** with a neutral thiol is not expected to take place. This is in line with the experimental findings that a reaction is not observed in organic solvents or neutral water/DMSO mixtures (**Section 2.6**) but only in a buffered medium. We also investigated if structures, which resemble the Meisenheimer complex, represent local minima on the potential surface. This is not the case as corresponding structures for the reaction with the thiol were found to be about 150 kJ/mol above the separated fragments. For the reaction with the thiolate, these were calculated to be more stable than the fragments but also do not represent local minima.

To elucidate possible mechanisms of buffer-mediated reactions, we modeled reactions in which possible buffer molecules act as intermediate storage for the thiol proton before transferring it to the sulfonyl leaving group. At the investigated pH of 7.5, the majority of the bicarbonate buffer is composed of HCO_3^- , but small fractions of CO_3^{2-} and H_2CO_3 are found as well. To include all these possibilities, we computed reaction paths for all protonation states of H_2CO_3 . The results are depicted in **Figure 9**. Besides the reaction paths, **Figure 9** depicts the variations in the geometrical arrangements for selected points along the reaction coordinate. Additional structures for the other paths can be found in **Supplementary Table S1**.

The reaction of methanethiol with HCO_3^- as buffer molecule shows an activation barrier of 56 kJ/mol which is significantly lower than the reaction barrier of the thiol without any buffer molecule (142 kJ/mol). The proton transfer to the buffer occurs at $R_{\text{thiol-C-2}_{\text{inhibitor}}} = 2.3 \text{ \AA}$. This point represents the top of the barrier. For the thiol, the top of the barrier is at about $R_{\text{thiol-C-2}_{\text{inhibitor}}} = 2.0 \text{ \AA}$. Neutral buffer molecules of H_2CO_3 are not able to bind the additional proton, hence no catalysis would be expected. Indeed, our computation predicted a reaction barrier of 124 kJ/mol, which lies only 20 kJ/mol below the barrier computed for unbuffered thiol (142 kJ/mol). CO_3^{2-} as buffer molecule facilitates a fast reaction with a barrier height of merely 24 kJ/mol. For this species, the proton transfer occurs earlier in the reaction at $R_{\text{thiol-C-2}_{\text{inhibitor}}} = 2.5 \text{ \AA}$. For the reaction catalyzed by HCO_3^- structures resembling the Meisenheimer complex are found to be about 50 kJ/mol higher in energy than the fragments, showing that no Meisenheimer complex is formed. These predictions that Meisenheimer complexes are energetically unfavorable supports the conclusion drawn by Hammett's analysis (**Section 2.7**).

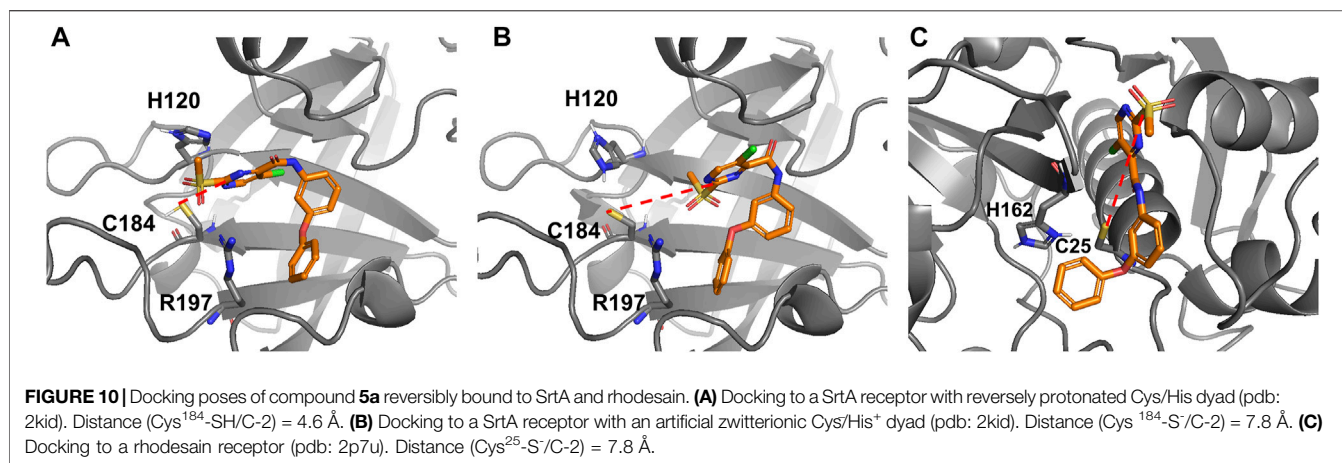


For further examination, the reaction paths for all phosphate buffer species were computed as well. The major component at pH 7.5 is HPO_4^{2-} , the computation yields an activation barrier of 31 kJ/mol, which is lower than that for HCO_3^- and comparable to the one found for CO_3^{2-} (**Supplementary Figure S6**). This could be confirmed experimentally since a faster reaction was observed by using a phosphate buffer instead of a bicarbonate buffer (**Section 2.6**). The H_2PO_4^- fraction of the phosphate buffer system shows a reaction barrier of 64 kJ/mol similar to the HCO_3^- mediated reaction.

To determine whether the reaction can occur *via* the His^{120} residue in SrtA, the model reaction path was calculated with 4-methylimidazole as a conjugated base, yielding a barrier height of 64 kJ/mol. Consequently, the inhibition reaction in presence of histidine could lead to a reaction path analogous to the reaction mediated by bicarbonate or phosphate buffers. Our computations indicate that thiolates would react with 2-sulfonylpyrimidines without any barrier while the reaction with thiol requires a base as a catalyst. This stands in contrast to the experimental finding that 2-sulfonylpyrimidines inhibit a reversely protonated Cys/His dyad in enzymes like SrtA (as shown in **Table 4**), but not enzymes with zwitterionic Cys/His⁺ dyad as cathepsin-like proteases (**Section 2.4**). According to Zhang et al. and our

model calculations, the nucleophilic reaction with a deprotonated cysteine residue should be preferred over the reaction with a neutral cysteine (Zhang et al., 2012). To address this question, we docked inhibitor **5a** to the SrtA receptors mimicking the zwitterionic and the neutral Cys/His dyads. The most advantageous docking poses are depicted in **Figures 10A,B**. For the neutral dyad, **5a** forms a quite stable complex blocking the active site. For the zwitterionic receptor, the inhibitor stays outside of the binding pocket with a distance ($\text{Cys}^{184}\text{-SH}/\text{C}-2$) = 7.8 Å. A similar result is found for the docking pose of inhibitor **5a** in the zwitterionic cathepsin-like protease rhodesain (**Figure 10C**) which also shows an enlarged $\text{Cys}^{25}\text{-S}/\text{C}-2$ distance of 7.8 Å.

Thus, the docking indicates that the possibility of a reaction does not result from the reactivity of the thiol or thiolate group but rather from the possibility to form an enzyme-inhibitor complex which can result in a covalent reaction. According to our findings for a zwitterionic dyad, the reaction would be very fast. However, it does not take place because the 2-sulfonylpyrimidine warhead does not fit into the active site due to unfavorable intermolecular interactions. For a neutral Cys/His dyad, the 2-sulfonylpyrimidine fits into the pocket, however, according to the experimental and theoretical



findings, a base catalyst is needed that acts as a proton buffer. Our computations show that the histidine could be this catalyst if it is sufficiently close. This role of His¹²⁰ as a proton buffer is supported by the fact that the inhibition potency decreases between pH 7.0 and 6.5 for which His¹²⁰ undergoes a significant protonation change (Connolly et al., 2003).

3 CONCLUSION

In summary, our investigations show that 2-sulfonylpyrimidines act as irreversible inhibitors for *S. aureus* SrtA possessing a neutral Cys/His dyad. Considerably weaker inhibition is found for enzymes with zwitterionic Cys/His⁺ dyads as found in cathepsin-like proteases. Inactivation measurements at higher pH values show no increase in the inhibitory potency of 2-sulfonylpyrimidines which, in this regard, stands in contrast to other known SrtA inhibitors. Measurements in solution show that no reaction takes place in a DMSO/water mixture. Only in presence of a buffer like bicarbonate or phosphate buffered solution (pH ~7.5), a reaction was observed.

While the enzyme inactivation measurements indicate that 2-sulfonylpyrimidines react preferentially with protonated thiols, the investigations of in-solution cysteine reactivity indicate that this reaction is hampered. To get a better understanding of these conflicting data, we performed quantum chemical model calculations in water/DMSO, bicarbonate, and phosphate buffers. Our computations predict that thiolates react with 2-sulfonylpyrimidines without any barrier. This is not the case for a protonated thiol for which a very high barrier of 142 kJ/mol is computed. The barrier is considerably lowered for bicarbonate or phosphate buffer solutions because the conjugated bases, e.g., HCO₃⁻, CO₃²⁻, act as base-catalysts. The barriers drop because these bases induce a proton transfer from the thiol, thus increasing the nucleophilicity of the attacking agent. As expected, the decrease of the barrier heights correlates with the basicity of the catalyst. Additional computations show that imidazole can also act as a catalyst. It reduces the reaction barrier from 142 kJ/mol to about 64 kJ/mol.

The computations predict that a deprotonated cysteine should react considerably more efficiently with 2-sulfonylpyrimidines than protonated cysteine moieties. In contrast, our enzyme inhibition measurements only show an efficient inhibition of SrtA with neutral Cys/His dyads while enzymes possessing a zwitterionic Cys/His⁺ dyad in their reactive center are less affected. This contradiction is resolved by docking studies, which predict that 2-sulfonylpyrimidines only enter the active sites of enzymes with neutral Cys/His dyads. If the dyad of SrtA is artificially switched to a Cys/His⁺ dyad, the 2-sulfonylpyrimidine does not fit the active site. For rhodensain, which possesses a zwitterionic Cys/His⁺ dyad, the same results are found. Intermolecular interactions prevent the formation of an enzyme-inhibitor complex whose geometrical arrangements allow the reaction. As a catalyst for the reaction of 2-sulfonylpyrimidines with SrtA, the His¹²⁰ moiety can act as a base catalyst. In line with the Hammett plots, our computations indicate that Meisenheimer complexes are energetically unfavorable for the energy surface of the S_NAr substitution reaction.

4 MATERIALS AND METHODS

4.1 Synthesis

Synthesis protocols of all compounds with their analytical data and the spectral appendix are provided in the supporting information.

4.2 Protein Expression and Purification

Expression of the *S. aureus* SrtA was performed as described previously (Schmohl et al., 2017a). The pET23b expression construct was transformed into *E. coli* strain BL21 Gold (DE3) cells (Agilent Technologies, Santa Clara, California) and grown in LB medium with 100 μM ampicillin at 37 °C to an OD₆₀₀ of ~0.7. Expression was then induced with 1 mM isopropyl- β -thiogalactoside (IPTG) for 16 h at 20 °C. Harvested cells were resuspended in lysis buffer (20 mM Tris HCl, pH 6.9, 300 mM NaCl, 0.1% Triton X-100, RNase, DNase, lysozyme) and lysed by multiple cycles of sonication (Sonoplus, Bandelin,

Berlin, Germany). After centrifugation (45 min at 15 krpm), the cleared lysate was subjected to IMAC (HisTrap HP 5 ml column, GE Healthcare, Chicago, Illinois) to isolate crude SrtA. For further purification, SrtA containing fractions were subsequently subjected to a gel-filtration step (HiLoad 16/60 Superdex 200 column, GE Healthcare) and eluted in the storage buffer (20 mM Tris-HCl, pH 7.50, 150 mM NaCl, 5 mM CaCl₂). For storage at -80°C, the pure SrtA was concentrated, aliquoted and shock frozen in liquid nitrogen. Throughout all steps, protein concentrations were determined *via* absorbance at 280 nm and sample purity was assessed *via* sodium dodecyl sulfate-polyacrylamide gel electrophoresis (SDS-PAGE).

4.3 Inhibition of Sortase A

Inhibition assays of *S. aureus* SrtA transpeptidation reactions were performed as described previously (Barthels et al., 2020). Briefly, the recombinantly expressed SrtA (final concentration: 1 μM) was incubated in assay buffer (50 mM Tris, 150 mM NaCl, 5 mM CaCl₂, pH 7.50) with 25 μM of the FRET-pair substrate Abz-LPETG-Dap (Dnp)-OH (Genscript, Piscataway, New Jersey) and 0.5 mM tetraglycine (Sigma Aldrich, St. Louis, Missouri). Inhibitors were added from DMSO stocks. Reactions were initiated by addition of SrtA and monitored for 30 min at 30°C in an Infinite M200 Pro plate reader with λ_{ex} 320 nm/λ_{em} 430 nm (Tecan, Männedorf, Switzerland). Three technical replicates were carried out for each inhibitor in black flat-bottom 96-well plates (Greiner bio-one, Kremsmünster, Austria). The enzyme kinetics of irreversible SrtA inactivation were analyzed as described previously (Barthels et al., 2020).

4.4 Protease Inhibition Selectivity

Fluorometric assays of the ZIKV/DENV NS2B/NS3 protease were performed as described previously (Maus et al., 2021). The assay was carried out in triplicates at 25°C in assay buffer (50 mM Tris, pH 9.0, 20% glycerol (v/v), and 1 mM CHAPS). 100 μM Boc-Gly-Arg-Arg-AMC (Bachem, Bubendorf, Switzerland) was used as a substrate. Fluorometric assays for cathepsin B, cathepsin L, and rhodesain (Calbiochem, Merck Millipore, Burlington, Massachusetts) were performed as described previously (Klein et al., 2020a). Cbz-Phe-Arg-AMC (Bachem, Bubendorf, Switzerland) was used as substrate (100 μM for cathepsin B, 6.5 μM for cathepsin L, and 10 μM for rhodesain). Fluorometric assays for urokinase plasminogen activator were performed as described previously (Angelini et al., 2012). 240 μM Cbz-Gly-Arg-Arg-AMC (Bachem, Bubendorf, Switzerland) was used as a substrate.

4.5 Mass Spectrometry

4.5.1 ESI-MS

To a solution of 100 μM cysteine in phosphate-buffered saline (1×, pH 7.5), compound **5a** or **7a** (100 μM, 5% DMSO) was added and incubated for 10 min at room temperature. The negative labeling control was performed by mock treatment with DMSO. Samples were analyzed by LC/MS using an Agilent 1100 series HPLC system with an Agilent Poroshell 120 EC-C18 column (150 × 2.10 mm 4 μm; mobile phase: ACN/H₂O 45:55 + 0.1% formic

acid; flow rate: 0.4 ml/min) and electron spray ionization with the Agilent 1100 series LC/MSD Trap in positive ionization mode.

4.5.2 MALDI-MS

An *S. aureus* SrtA stock solution was diluted in 100 μL assay buffer (50 mM Tris, 150 mM NaCl, 5 mM CaCl₂, pH 7.50) to a final concentration of 10 μM. Compound **7a** was dissolved in DMSO and added to SrtA at a final concentration of 100 μM. The protein samples were allowed to react for 1 h at room temperature and subsequently, these were desalted using ZebaTM Spin desalting columns (7 kDa MWCO, 0.5 ml; Thermo Scientific) according to the manufacturer's instructions. For MALDI sample preparation, the desalted solution was mixed 1:1 with a matrix combination of equal amounts α-cyano-4-hydroxycinnamic acid (20 mg/ml dissolved in 70% acetonitrile and 30% of formic acid in water at a concentration of 5%) and 2,5-dihydroxybenzoic acid (20 mg/ml dissolved in 70% acetonitrile and 30% of trifluoroacetic acid in water at a concentration of 0.1%). The resulting mixture was allowed to dry slowly on the MALDI target prior to introduction into the mass spectrometer. The measurements were carried out on a rapiflexTM MALDI-TOF/TOF mass spectrometer (Bruker Daltonik GmbH, Bremen, Germany). The instrument is equipped with a scanning smartbeam 10 kHz Nd:YAG laser at a wavelength of 355 nm and a 10 bit 5 GHz digitizer. The acceleration voltage was set to 20 kV and the mass spectra were recorded in positive ion linear mode. Calibration was done with the Bruker protein calibration standard II in a mass range from 10 to 70 kDa. Samples were measured at a laser power of 60% with random walk ionization across the sample spot.

4.6 Cysteine Reactivity Assay

Kinetic characterization of the reaction between sulfonylpyrimidines and cysteine was performed in degassed phosphate buffer (1×PBS, pH 7.5) or individual cases in bicarbonate buffer (20 mM NaHCO₃, 100 mM NaCl, pH 7.5). Three technical replicates were carried out for each sulfonylpyrimidine in black flat-bottom 96-well plates. For this purpose, 50 μL buffered solution (including 5% (v/v) DMSO) of the respective sulfonylpyrimidine derivative (final: 250–3 μM) and the cysteine reactive probe **8** (final: 5 μM) were premixed. Reactions were initiated by the addition of 50 μL cysteine (final: 5 μM), dissolved in the respective buffer, and monitored for 30 min at 30°C in an Infinite M200 Pro plate reader with λ_{ex} 380 nm/λ_{em} 460 nm. To calculate *k*_{obs} and *k*_{chem} values, fluorescence curves were fitted using the same non-linear regression as for *in vitro* inhibition of SrtA (Barthels et al., 2020).

4.7 Molecular Modeling

JChem for Office (Excel) was used for the virtual synthesis of an in-house docking library. JChem for Office 20.18.0, 2020, ChemAxon (<http://www.chemaxon.com>) (Bode, 2004). For this purpose, a database of 438 in-house available amine building blocks was amide-coupled *in silico* with the sulfonylpyrimidine carboxylic acid **5c**. The resulting product structures were exported in the SDF file format. For virtual screening of this compound library, a Glide docking protocol was conducted

within the Schrödinger Maestro 2020.04 worksuite (Friesner et al., 2004). The protein structures pdb: 2kid (frame 1, SrtA) and 2p7u (rhodesain) were downloaded from the Protein Databank (PDB). Before docking, the alkylated active-site Cys¹⁸⁴ (SrtA) or Cys²⁵ (rhodesain) were untethered and reprotonated. Receptor preparation was performed using the automated binding site, protonation, and energy minimization routine within Maestro “Protein preparation” and “Receptor grid generation.” Ligands were energy minimized using the “LigPrep” routine. The docking protocol was performed under default parameters with extra precision (XP) settings. Subsequently, predicted binding modes were analyzed to select the most promising candidate compounds for wet-lab synthesis. Ranking of the virtual screening output was performed according to the total docking score and in a second step according to the predicted binding mode (i.e., positioning and distance of the warhead relative to the Cys¹⁸⁴).

4.8 Quantum Chemical Methods

All calculations were carried out with the Gaussian16 program (Frisch et al., 2020). The DFT functional B3LYP (Vosko et al., 1980; Lee et al., 1988; Becke, 1993) with Grimme’s D3 correction (Grimme et al., 2010) and the Pople basis set 6-31+G (d,p) were employed. Implicit solvation in water was included with the SMD solvation method (Marenich et al., 2009). The geometry of the reactants was optimized to obtain the starting structures. Subsequently, a scan was performed in which the distance of the methanethiol (ate) to the attacking carbon atom of the inhibitor (C-2) was gradually shortened. Reaction profiles were calculated for the reaction of the inhibitor with methanethiolate, methanethiol, and with methanethiol in presence of a buffer molecule. As buffer molecules, all species of the bicarbonate buffer and phosphate buffer species, respectively, were considered. For the reaction of the thiolate anion with the inhibitor, the dihedral angle between the thiolate carbon, thiolate sulfur, C-2 and C-5 of the inhibitor was frozen, because otherwise the thiolate was not oriented towards the attacking carbon. However, for the distances $R(S_{\text{thiolate}}-C-2_{\text{inhibitor}}) = 1.8/1.9 \text{ \AA}$ the restraint was removed to ensure the correct product geometry. Reactants

and products were confirmed by calculations without restraints and frequency calculations.

DATA AVAILABILITY STATEMENT

The original contributions presented in the study are included in the article/**Supplementary Material**, further inquiries can be directed to the corresponding author.

AUTHOR CONTRIBUTIONS

TS, BE, WZ, and FB conceived and designed the research; FB, JM, SH, and H-JR performed the research; FB, JM, TM, and BE analyzed the data; FB, BE, JM, TS, and SH wrote the manuscript. The final manuscript has been seen and approved by all authors, and we have taken due care to ensure the integrity of the work.

FUNDING

The work of WZ is funded by the German Research Council (DFG) ShARE (ZI665/3-1) and the German Federal Ministry of Education and Research (BMBF) (16GW0297).

ACKNOWLEDGMENTS

We thank Prof. Dirk Schwarzer (University of Tuebingen) for providing the expression plasmid of *S. aureus* SrtA. The authors gratefully acknowledge ChemAxon Ltd. for the donation of the academic license to the JChem package.

SUPPLEMENTARY MATERIAL

The Supplementary Material for this article can be found online at: <https://www.frontiersin.org/articles/10.3389/fmolb.2021.804970/full#supplementary-material>

REFERENCES

- Allen, R. C., Popat, R., Diggle, S. P., and Brown, S. P. (2014). Targeting Virulence: Can We Make Evolution-Proof Drugs? *Nat. Rev. Microbiol.* 12, 300–308. doi:10.1038/nrmicro3232
- Angelini, A., Cendron, L., Chen, S., Touati, J., Winter, G., Zanotti, G., et al. (2012). Bicyclic Peptide Inhibitor Reveals Large Contact Interface with a Protease Target. *ACS Chem. Biol.* 7, 817–821. doi:10.1021/cb200478t
- Awoonor-Williams, E., and Rowley, C. N. (2018). How Reactive Are Druggable Cysteines in Protein Kinases? *J. Chem. Inf. Model.* 58, 1935–1946. doi:10.1021/acs.jcim.8b00454
- Bajorath, J. (2019). Duality of Activity Cliffs in Drug Discovery. *Expert Opin. Drug Discov.* 14, 517–520. doi:10.1080/17460441.2019.1593371
- Barthels, F., Marincola, G., Marciniak, T., Konhäuser, M., Hammerschmidt, S., Bierlmeier, J., et al. (2020). Asymmetric Disulfanylbenzamidates as Irreversible and Selective Inhibitors of *Staphylococcus aureus* Sortase A. *ChemMedChem* 15, 839–850. doi:10.1002/cmdc.201900687
- Bauer, M. R., Joerger, A. C., and Fersht, A. R. (2016). 2-Sulfonylpyrimidines: Mild Alkylating Agents with Anticancer Activity toward P53-Compromised Cells. *Proc. Natl. Acad. Sci. USA* 113, E5271–E5280. doi:10.1073/pnas.1610421113
- Becke, A. D. (1993). Density-functional Thermochemistry. III. The Role of Exact Exchange. *J. Chem. Phys.* 98, 5648–5652. doi:10.1063/1.464913
- Bentley, M. L., Lamb, E. C., and McCafferty, D. G. (2008). Mutagenesis Studies of Substrate Recognition and Catalysis in the Sortase A Transpeptidase from *Staphylococcus aureus*. *J. Biol. Chem.* 283, 14762–14771. doi:10.1074/jbc.M800974200
- Bode, J. W. (2004). *Reactor ChemAxon Ltd.* Maramaros koz 2/a. Budapest, 1037 Hungary: ChemAxon. Available at: www.chemaxon.com.
- Böhme, A., Thaens, D., Paschke, A., and Schüürmann, G. (2009). Kinetic Glutathione Chemoassay to Quantify Thiol Reactivity of Organic Electrophiles—Application to α,β -Unsaturated Ketones, Acrylates, and Propiolates. *Chem. Res. Toxicol.* 22, 742–750. doi:10.1021/tx800492x
- Bradshaw, W. J., Davies, A. H., Chambers, C. J., Roberts, A. K., Shone, C. C., and Acharya, K. R. (2015). Molecular Features of the Sortase Enzyme Family. *FEBS J.* 282, 2097–2114. doi:10.1111/febs.13288

- Buděšínský, Z., and Vavřina, J. (1972). Nucleophilic Substitutions in the 2-methanesulfonylpyrimidine Series. *Collect. Czech. Chem. Commun.* 37, 1721–1733. doi:10.1135/cccc19721721
- Cascioferro, S., Raffa, D., Maggio, B., Raimondi, M. V., Schillaci, D., and Daidone, G. (2015). Sortase A Inhibitors: Recent Advances and Future Perspectives. *J. Med. Chem.* 58, 9108–9123. doi:10.1021/acs.jmedchem.5b00779
- Cascioferro, S., Totsika, M., and Schillaci, D. (2014). Sortase A: An Ideal Target for Anti-virulence Drug Development. *Microb. Pathogenesis* 77, 105–112. doi:10.1016/j.micpath.2014.10.007
- Chan, A. H., Yi, S. W., Weiner, E. M., Amer, B. R., Sue, C. K., Wereszczynski, J., et al. (2017). NMR Structure-Based Optimization of Staphylococcus Aureus Sortase A Pyridazine Inhibitors. *Chem. Biol. Drug Des.* 90, 327–344. doi:10.1111/cbdd.12962
- Chipinda, I., Ajibola, R. O., Morakinyo, M. K., Ruwona, T. B., Simoyi, R. H., and Siegel, P. D. (2010). Rapid and Simple Kinetics Screening Assay for Electrophilic Dermal Sensitizers Using Nitrobenzenethiol. *Chem. Res. Toxicol.* 23, 918–925. doi:10.1021/tx100003w
- Choi, Hojune., Lee, Jong-Pal., Park, Jong. Keun., Yang, Kiyull., and Koo, In. Sun. (2009). Kinetic Studies on the Nucleophilic Substitution Reaction of 4-X-Substituted-2,6-Dinitrochlorobenzene with Pyridines in MeOH-MeCN Mixtures. *Bull. Korean Chem. Soc.* 30, 1579–1582. doi:10.5012/BKCS.2009.30.7.1579
- Clancy, K. W., Melvin, J. A., and McCafferty, D. G. (2010). Sortase Transpeptidases: Insights into Mechanism, Substrate Specificity, and Inhibition. *Biopolymers* 94, 385–396. doi:10.1002/bip.21472
- Connolly, K. M., Smith, B. T., Pilpa, R., Ilangovan, U., Jung, M. E., and Clubb, R. T. (2003). Sortase from *Staphylococcus aureus* Does Not Contain a Thiolate-Imidazolium Ion Pair in its Active Site. *J. Biol. Chem.* 278, 34061–34065. doi:10.1074/jbc.M305245200
- Copeland, R. A. (2005). *Evaluation of Enzyme Inhibitors in Drug Discovery: A Guide for Medicinal Chemists and Pharmacologists*. Second Edition. Hoboken, NJ: John Wiley & Sons, 572. doi:10.1002/9781118540398
- Dickey, S. W., Cheung, G. Y. C., and Otto, M. (2017). Different Drugs for Bad Bugs: Antivirulence Strategies in the Age of Antibiotic Resistance. *Nat. Rev. Drug Discov.* 16, 457–471. doi:10.1038/nrd.2017.23
- Ehmke, V., Winkler, E., Banner, D. W., Haap, W., Schweizer, W. B., Rottmann, M., et al. (2013). Optimization of Triazine Nitriles as Rhodocin Inhibitors: Structure-Activity Relationships, Bioisosteric Imidazopyridine Nitriles, and X-ray Crystal Structure Analysis with Human Cathepsin L. *ChemMedChem* 8, 967–975. doi:10.1002/cmdc.201300112
- Epps, D. E., and Taylor, B. M. (2001). A Competitive Fluorescence Assay to Measure the Reactivity of Compounds. *Anal. Biochem.* 295, 101–106. doi:10.1006/abio.2001.5173
- Flynn, G. L. (1980). Substituent Constants for Correlation Analysis in Chemistry and Biology. *J. Pharm. Sci.* 69, 1109. doi:10.1002/jps.2600690938
- Förster, T., Shang, E., Shimizu, K., Sanada, E., Schölermann, B., Huebner, M., et al. (2019). 2-Sulfonylpyrimidines Target the Kinesin HSET via Cysteine Alkylation. *Eur. J. Org. Chem.* 2019, 5486–5496. doi:10.1002/ejoc.201900586
- Frankel, B. A., Kruger, R. G., Robinson, D. E., Kelleher, N. L., and McCafferty, D. G. (2005). *Staphylococcus aureus* Sortase Transpeptidase SrtA: Insight into the Kinetic Mechanism and Evidence for a Reverse Protonation Catalytic Mechanism. *Biochemistry* 44, 11188–11200. doi:10.1021/bi050141j
- Friesner, R. A., Banks, J. L., Murphy, R. B., Halgren, T. A., Klicic, J. J., Mainz, D. T., et al. (2004). Glide: A New Approach for Rapid, Accurate Docking and Scoring. 1. Method and Assessment of Docking Accuracy. *J. Med. Chem.* 47, 1739–1749. doi:10.1021/jm0306430
- Frisch, M. J., Trucks, G. W., Schlegel, H. B., Scuseria, G. E., Robb, M. A., Cheeseman, J. R., et al. (2020). *Gaussian 16, Revision C. 01*. Wallingford CT: Gaussian, Inc.
- Grimme, S., Antony, J., Ehrlich, S., and Krieg, H. (2010). A Consistent and Accurate Ab Initio Parametrization of Density Functional Dispersion Correction (DFT-D) for the 94 Elements H-Pu. *J. Chem. Phys.* 132, 154104. doi:10.1063/1.3382344
- Hallenbeck, K., Turner, D., Renslo, A., and Arkin, M. (2016). Targeting Non-catalytic Cysteine Residues through Structure-Guided Drug Discovery. *Ctmc* 17, 4–15. doi:10.2174/1568026616666160719163839
- Hammett, L. P. (1937). The Effect of Structure upon the Reactions of Organic Compounds. Benzene Derivatives. *J. Am. Chem. Soc.* 59, 96–103. doi:10.1021/ja01280a022
- Ilangovan, U., Ton-That, H., Iwahara, J., Schneewind, O., and Clubb, R. T. (2001). Structure of Sortase, the Transpeptidase that Anchors Proteins to the Cell wall of *Staphylococcus aureus*. *Proc. Natl. Acad. Sci.* 98, 6056–6061. doi:10.1073/pnas.101064198
- Jaudzems, K., Kurbatska, V., Jekabsons, A., Bobrovs, R., Rudevica, Z., and Leonchiks, A. (2020). Targeting Bacterial Sortase A with Covalent Inhibitors: 27 New Starting Points for Structure-Based Hit-To-Lead Optimization. *ACS Infect. Dis.* 6, 186–194. doi:10.1021/acinfecdis.9b00265
- Kappel, K., Wereszczynski, J., Clubb, R. T., and McCammon, J. A. (2012). The Binding Mechanism, Multiple Binding Modes, and Allosteric Regulation of *Staphylococcus aureus* Sortase A Probed by Molecular Dynamics Simulations. *Protein Sci.* 21, 1858–1871. doi:10.1002/pro.2168
- Kiemele, E. R., Wathier, M., Bichler, P., and Love, J. A. (2016). Total Synthesis of K777: Successful Application of Transition-Metal-Catalyzed Alkyne Hydrothiolation toward the Modular Synthesis of a Potent Cysteine Protease Inhibitor. *Org. Lett.* 18, 492–495. doi:10.1021/acs.orglett.5b03535
- Klein, P., Barthels, F., Johe, P., Wagner, A., Tenzer, S., Distler, U., et al. (2020a). Naphthoquinones as Covalent Reversible Inhibitors of Cysteine Proteases—Studies on Inhibition Mechanism and Kinetics. *Molecules* 25, 2064. doi:10.3390/molecules25092064
- Klein, P., Johe, P., Wagner, A., Jung, S., Kühlborn, J., Barthels, F., et al. (2020b). New Cysteine Protease Inhibitors: Electrophilic (Het)arenes and Unexpected Prodrug Identification for the Trypanosoma Protease Rhodocin. *Molecules* 25, 1451. doi:10.3390/molecules25061451
- Kruger, R. G., Barkallah, S., Frankel, B. A., and McCafferty, D. G. (2004a). Inhibition of the *Staphylococcus aureus* Sortase Transpeptidase SrtA by Phosphinic Peptidomimetics. *Bioorg. Med. Chem.* 12, 3723–3729. doi:10.1016/j.bmc.2004.03.066
- Kruger, R. G., Dostal, P., and McCafferty, D. G. (2004b). Development of a High-Performance Liquid Chromatography Assay and Revision of Kinetic Parameters for the *Staphylococcus aureus* Sortase Transpeptidase SrtA. *Anal. Biochem.* 326, 42–48. doi:10.1016/j.ab.2003.10.023
- Lee, C., Yang, W., and Parr, R. G. (1988). Development of the Colle-Salvetti Correlation-Energy Formula into a Functional of the Electron Density. *Phys. Rev. B* 37, 785–789. doi:10.1103/PhysRevB.37.785
- Li, L., Jiang, X., Huang, S., Ying, Z., Zhang, Z., Pan, C., et al. (2017a). Discovery of Highly Potent 2-Sulfonyl-Pyrimidinyl Derivatives for Apoptosis Inhibition and Ischemia Treatment. *ACS Med. Chem. Lett.* 8, 407–412. doi:10.1021/acsmchemlett.6b00489
- Li, Y., Phoo, W. W., Loh, Y. R., Zhang, Z., Ng, E. Y., Wang, W., et al. (2017b). Structural Characterization of the Linked NS2B-NS3 Protease of Zika Virus. *FEBS Lett.* 591, 2338–2347. doi:10.1002/1873-3468.12741
- Liew, C. K., Smith, B. T., Pilpa, R., Suree, N., Ilangovan, U., Connolly, K. M., et al. (2004). Localization and Mutagenesis of the Sorting Signal Binding Site on Sortase A from *Staphylococcus aureus*. *FEBS Lett.* 571, 221–226. doi:10.1016/j.febslet.2004.06.070
- Lyu, H., Petukhov, P. A., Banta, P. R., Jadhav, A., Lea, W. A., Cheng, Q., et al. (2020). Characterization of Lead Compounds Targeting the Selenoprotein Thioredoxin Glutathione Reductase for Treatment of Schistosomiasis. *ACS Infect. Dis.* 6, 393–405. doi:10.1021/acinfecdis.9b00354
- Marenich, A. V., Cramer, C. J., and Truhlar, D. G. (2009). Universal Solvation Model Based on Solute Electron Density and on a Continuum Model of the Solvent Defined by the Bulk Dielectric Constant and Atomic Surface Tensions. *J. Phys. Chem. B* 113, 6378–6396. doi:10.1021/jp810292n
- Maresso, A. W., Wu, R., Kern, J. W., Zhang, R., Janik, D., Missiakas, D. M., et al. (2007). Activation of Inhibitors by Sortase Triggers Irreversible Modification of the Active Site. *J. Biol. Chem.* 282, 23129–23139. doi:10.1074/jbc.M701857200
- Maus, H., Barthels, F., Hammerschmidt, S. J., Kopp, K., Millies, B., Gellert, A., et al. (2021). SAR of Novel Benzothiazoles Targeting an Allosteric Pocket of DENV and ZIKV NS2B/NS3 Proteases. *Bioorg. Med. Chem.* 47, 116392. doi:10.1016/j.bmc.2021.116392
- Mazmanian, S. K., Liu, G., Jensen, E. R., Lenoy, E., and Schneewind, O. (2000). *Staphylococcus aureus* Sortase Mutants Defective in the Display of Surface Proteins and in the Pathogenesis of Animal Infections. *Proc. Natl. Acad. Sci.* 97, 5510–5515. doi:10.1073/pnas.080520697

- Mazmanian, S. K., Liu, G., Ton-That, H., and Schneewind, O. (1999). *Staphylococcus aureus* Sortase, an Enzyme that Anchors Surface Proteins to the Cell Wall. *Science* 285, 760–763. doi:10.1126/science.285.5428.760
- Mladenovic, M., Schirmeister, T., Thiel, S., Thiel, W., and Engels, B. (2007). The Importance of the Active Site Histidine for the Activity of Epoxide- or Aziridine-Based Inhibitors of Cysteine Proteases. *ChemMedChem* 2, 120–128. doi:10.1002/cmdc.200600159
- Mu, D., Xiang, H., Dong, H., Wang, D., and Wang, T. (2018). Isoviteixin, a Potential Candidate Inhibitor of Sortase A of *Staphylococcus aureus* USA300. *J. Microbiol. Biotechnol.* 28, 1426–1432. doi:10.4014/jmb.1802.02014
- Otto, H.-H., and Schirmeister, T. (1997). Cysteine Proteases and Their Inhibitors. *Chem. Rev.* 97, 133–172. doi:10.1021/cr950025u
- Paasche, A., Zipper, A., Schäfer, S., Ziebuhr, J., Schirmeister, T., and Engels, B. (2014). Evidence for Substrate Binding-Induced Zwitterion Formation in the Catalytic Cys-His Dyad of the SARS-CoV Main Protease. *Biochemistry* 53, 5930–5946. doi:10.1021/bi400604t
- Perry, A. M., Ton-That, H., Mazmanian, S. K., and Schneewind, O. (2002). Anchoring of Surface Proteins to the Cell Wall of *Staphylococcus aureus*. *J. Biol. Chem.* 277, 16241–16248. doi:10.1074/jbc.M109194200
- Rohrbach, S., Smith, A. J., Pang, J. H., Poole, D. L., Tuttle, T., Chiba, S., et al. (2019). Concerted Nucleophilic Aromatic Substitution Reactions. *Angew. Chem. Int. Ed.* 58, 16368–16388. doi:10.1002/anie.201902216
- Sameshima, T., Miyahisa, I., Yamasaki, S., Gotou, M., Kobayashi, T., and Sakamoto, J. (2017). High-Throughput Quantitative Intrinsic Thiol Reactivity Evaluation Using a Fluorescence-Based Competitive Endpoint Assay. *SLAS DISCOVERY: Advancing Sci. Drug Discov.* 22, 1168–1174. doi:10.1177/2472555217704654
- Schmohl, L., Bierlmeier, J., Gerth, F., Freund, C., and Schwarzer, D. (2017a). Engineering Sortase A by Screening a Second-Generation Library Using Phage Display. *J. Pept. Sci.* 23, 631–635. doi:10.1002/psc.2980
- Schmohl, L., Bierlmeier, J., von Kügelgen, N., Kurz, L., Reis, P., Barthels, F., et al. (2017b). Identification of Sortase Substrates by Specificity Profiling. *Bioorg. Med. Chem.* 25, 5002–5007. doi:10.1016/j.bmc.2017.06.033
- Schmohl, L., Wagner, F. R., Schümann, M., Krause, E., and Schwarzer, D. (2015). Semisynthesis and Initial Characterization of Sortase A Mutants Containing Selenocysteine and Homocysteine. *Bioorg. Med. Chem.* 23, 2883–2889. doi:10.1016/j.bmc.2015.03.057
- Schneewind, O., and Missiakas, D. (2019). Sortases, Surface Proteins, and Their Roles in *Staphylococcus aureus* Disease and Vaccine Development. *Protein Secret. Bact.* 7, 173–188. doi:10.1128/microbiolspec.PSIB-0004-201810.1128/9781683670285.ch15
- Schoonen, W. G. E. J., Westerink, W. M. A., de Roos, J. A. D. M., and Débiton, E. (2005). Cytotoxic Effects of 100 Reference Compounds on Hep G2 and HeLa Cells and of 60 Compounds on ECC-1 and CHO Cells. I Mechanistic Assays on ROS, Glutathione Depletion and Calcein Uptake. *Toxicol. Vitro* 19, 505–516. doi:10.1016/j.tiv.2005.01.003
- Scott, C. J., McDowell, A., Martin, S. L., Lynas, J. F., Vandenbroeck, K., and Walker, B. (2002). Irreversible Inhibition of the Bacterial Cysteine Protease-Transpeptidase Sortase (SrtA) by Substrate-Derived Affinity Labels. *Biochem. J.* 366, 953–958. doi:10.1042/bj20020602
- Sprague, J. M., and Johnson, T. B. (1936). Researches on Pyrimidines. CXLIX. Reactions of Some 2-Ethylsulfonypyrimidines. *J. Am. Chem. Soc.* 58, 423–426. doi:10.1021/ja01294a010
- Suree, N., Liew, C. K., Villareal, V. A., Thieu, W., Fadeev, E. A., Clemens, J. J., et al. (2009a). The Structure of the *Staphylococcus aureus* Sortase-Substrate Complex Reveals How the Universally Conserved LPXTG Sorting Signal Is Recognized. *J. Biol. Chem.* 284, 24465–24477. doi:10.1074/jbc.M109.022624
- Suree, N., Yi, S. W., Thieu, W., Marohn, M., Damoiseaux, R., Chan, A., et al. (2009b). Discovery and Structure-Activity Relationship Analysis of *Staphylococcus aureus* Sortase A Inhibitors. *Bioorg. Med. Chem.* 17, 7174–7185. doi:10.1016/j.bmc.2009.08.067
- Ton-That, H., Liu, G., Mazmanian, S. K., Faull, K. F., and Schneewind, O. (1999). Purification and Characterization of Sortase, the Transpeptidase that Cleaves Surface Proteins of *Staphylococcus aureus* at the LPXTG Motif. *Proc. Natl. Acad. Sci.* 96, 12424–12429. doi:10.1073/pnas.96.22.12424
- Ton-That, H., Mazmanian, S. K., Alksne, L., and Schneewind, O. (2002). Anchoring of Surface Proteins to the Cell Wall of *Staphylococcus aureus*. *J. Biol. Chem.* 277, 7447–7452. doi:10.1074/jbc.M109945200
- Ton-That, H., and Schneewind, O. (1999). Anchor Structure of Staphylococcal Surface Proteins. *J. Biol. Chem.* 274, 24316–24320. doi:10.1074/jbc.274.34.24316
- Tsompanidou, E., Denham, E. L., Sibbald, M. J. J. B., Yang, X.-m., Seinen, J., Friedrich, A. W., et al. (2012). The Sortase A Substrates FnbpA, FnbpB, ClfA and ClfB Antagonize Colony Spreading of *Staphylococcus aureus*. *PLoS One* 7, e44646. doi:10.1371/journal.pone.0044646
- van't Hof, W., Maňásková, S. H., Veerman, E. C. I., and Bolscher, J. G. M. (2015). Sortase-mediated Backbone Cyclization of Proteins and Peptides. *Biol. Chem.* 396, 283–293. doi:10.1515/hsz-2014-0260
- Vosko, S. H., Wilk, L., and Nusair, M. (1980). Accurate Spin-dependent Electron Liquid Correlation Energies for Local Spin Density Calculations: a Critical Analysis. *Can. J. Phys.* 58, 1200–1211. doi:10.1139/p80-159
- Webb, K. S. (1994). A Mild, Inexpensive and Practical Oxidation of Sulfides. *Tetrahedron Lett.* 35, 3457–3460. doi:10.1016/S0040-4039(00)73209-6
- Wehrli, P. M., Uzelac, I., Olsson, T., Jacso, T., Tietze, D., and Gottfried, J. (2019). Discovery and Development of Substituted Thiadiazoles as Inhibitors of *Staphylococcus aureus* Sortase A. *Bioorg. Med. Chem.* 27, 115043. doi:10.1016/j.bmc.2019.115043
- Weiss, W. J., Lenoy, E., Murphy, T., Tardio, L., Burgio, P., Projan, S. J., et al. (2004). Effect of srtA and srtB Gene Expression on the Virulence of *Staphylococcus aureus* in Animal Models of Infection. *J. Antimicrob. Chemother.* 53, 480–486. doi:10.1093/jac/dkh078
- Wilke, J., Kawamura, T., Watanabe, N., Osada, H., Ziegler, S., and Waldmann, H. (2018). Identification of Cytotoxic, Glutathione-Reactive Moieties Inducing Accumulation of Reactive Oxygen Species via Glutathione Depletion. *Bioorg. Med. Chem.* 26, 1453–1461. doi:10.1016/j.bmc.2017.11.009
- Yang, T., Zhang, T., Guan, X.-N., Dong, Z., Lan, L., Yang, S., et al. (2020). Tideglusib and its Analogues as Inhibitors of *Staphylococcus aureus* SrtA. *J. Med. Chem.* 63, 8442–8457. doi:10.1021/acs.jmedchem.0c00803
- Zeng, R.-F., Lan, J.-S., Li, X.-D., Liang, H.-F., Liao, Y., Lu, Y.-J., et al. (2017). A Fluorescent Coumarin-Based Probe for the Fast Detection of Cysteine with Live Cell Application. *Molecules* 22, 1618. doi:10.3390/molecules22101618
- Zhang, D., Devarie-Baez, N. O., Li, Q., Lancaster, J. R., and Xian, M. (2012). Methylsulfonyl Benzothiazole (MSBT): A Selective Protein Thiol Blocking Reagent. *Org. Lett.* 14, 3396–3399. doi:10.1021/ol301370s
- Zhang, J., Liu, H., Zhu, K., Gong, S., Dramsi, S., Wang, Y.-T., et al. (2014). Anti-infective Therapy with a Small Molecule Inhibitor of *Staphylococcus aureus* Sortase A. *Proc. Natl. Acad. Sci. USA* 111, 13517–13522. doi:10.1073/pnas.1408601111
- Zhulenkovs, D., Rudevica, Z., Jaudzems, K., Turks, M., and Leonchiks, A. (2014). Discovery and Structure-Activity Relationship Studies of Irreversible Benzisothiazolinone-Based Inhibitors against *Staphylococcus aureus* Sortase A Transpeptidase. *Bioorg. Med. Chem.* 22, 5988–6003. doi:10.1016/j.bmc.2014.09.011
- Zong, Y., Bice, T. W., Ton-That, H., Schneewind, O., and Narayana, S. V. L. (2004). Crystal Structures of *Staphylococcus aureus* Sortase A and its Substrate Complex. *J. Biol. Chem.* 279, 31383–31389. doi:10.1074/jbc.M401374200

Conflict of Interest: The authors declare that the research was conducted in the absence of any commercial or financial relationships that could be construed as a potential conflict of interest.

Publisher's Note: All claims expressed in this article are solely those of the authors and do not necessarily represent those of their affiliated organizations, or those of the publisher, the editors, and the reviewers. Any product that may be evaluated in this article, or claim that may be made by its manufacturer, is not guaranteed or endorsed by the publisher.

Copyright © 2022 Barthels, Meyr, Hammerschmidt, Marciniak, Räder, Ziebuhr, Engels and Schirmeister. This is an open-access article distributed under the terms of the Creative Commons Attribution License (CC BY). The use, distribution or reproduction in other forums is permitted, provided the original author(s) and the copyright owner(s) are credited and that the original publication in this journal is cited, in accordance with accepted academic practice. No use, distribution or reproduction is permitted which does not comply with these terms.